The Pennsylvania State University
The Graduate School

VISION-BASED DECK STATE ESTIMATION FOR AUTONOMOUS SHIP-BOARD LANDING

A Thesis in
Aerospace Engineering
by
Benjamin L. Truskin

Submitted in Partial Fulfillment
of the Requirements
for the Degree of

Master of Science

May 2013

The thesis of Benjamin L. Truskin was reviewed and approved* by the following:

Jacob W. Langelaan
Associate Professor of Aerospace Engineering
Thesis Advisor

Joseph F. Horn
Associate Professor of Aerospace Engineering

George A. Lesieutre
Professor of Aerospace Engineering
Head of the Department of Aerospace Engineering

*Signatures are on file in the Graduate School.

Abstract

Piloted landings on ship decks are a daunting challenge where life critical missions require operations to continue even under adverse conditions. Automating the landing process for a helicopter on any landing site would create a safer environment in many applications. The research detailed in this thesis was motivated by an even more difficult and specific situation: attempted landing of a small, payload limited UAV on a moving, non-cooperative or mildly cooperative ship deck. While current capabilities do include landing an autonomous rotorcraft onto a moving deck, this can only be performed under very restrictive conditions involving a cooperative ship deck and calm seas. The goal for this system is to have the generality necessary to successfully operate in a variety of sea conditions, and with many potential ship types.

This thesis details the development and simulation demonstration of a state estimation system that only requires the use of a monocular camera, an inertial measurement unit, and GPS. The INS/GPS is required to determine vehicle states. The camera provides information about landmark bearings relative to the UAV, but nothing else. By combining these two sensor systems, it is possible to estimate deck state, thus enabling the ability to autonomously land. This thesis presents Unscented Kalman Filter based implementation that utilizes a generic 2^{nd} order kinematic model driven by zero mean Gaussian noise for the ship deck motion model. Use of this generic model contains unmodeled dynamics, but is not particular to any ship.

The goal is to estimate position, attitude, velocity, and angular velocity for the deck. Estimator performance is reviewed using single run and multiple Monte Carlo simulations where the deck is subjected to a variety of wave conditions and various wave modeling techniques.

Table of Contents

List of Figures

List of Tables

List of Symbols

It is important to note that there is a convention for the naming of vectors and matrices. In this thesis all matrices shall be denoted as bold capital letters, while all vectors are denoted as bold lowercase letters. Any symbol with a hat over it is an estimate. Also any variable with a dot over it is a time derivative of that symbol.

All symbols, whether defined here or not, are defined at the point of first use for reader convenience as well.

γ	Denotes an angle measurement for given marker, p. 9
L	Denotes a fiducial marker, p. 9
$\mathbf{x}$	Denotes a state vector, p. 16
$[x\ y\ z]$	Denotes position states, p. 16
$[\phi\ \theta\ \psi]$	Denotes rotation angles states, p. 16
$[u\ v\ w]$	Denotes velocity states, p. 16
$[p\ q\ r]$	Denotes rotation rate states, p. 16
$\hat{\mathbf{x}}$	Denotes a state estimate, p. 17
$\hat{\mathbf{P}}$	Denotes an estimate covariance matrix, p. 17
$\mathbf{u}$	Denotes light position, p. 17
$\mathbf{T}$	Denotes a rotation matrix, p. 19
$\mathbf{s}_i$	Denotes the relative distance from the light to the camera, p. 21
$\mathbf{x}_i$	Denotes light position, p. 22
F_d	Denotes wave force acting upon deck, p. 22

Acknowledgments

When I first started on my Masters Degree I was nervous. I had been a student for the majority of my life, but now being relied on to produce research and results on top of academics was a scary prospect. I am happy to say the experience has gone better than I could have hoped, and there are several people I'd like to thank for that.

My first thanks has to go out to my advisor Jack Langelaan. He took what was a massive multiyear project and broke it down into bite size bits that I could digest and not find too overwhelming. His experience kept me from wasting too much of my time, and accomplishing the goals we set out two years ago for my thesis.

In that same thought I must also thank everyone down in the AVIA lab that helped me when I was stuck. I would of been lost and confused many times had it not been for the guidance and assistance provided by Sean Marlow, Nate Depenbusch, John Quindlen, Shawn Daugherty, Zuqun Li and everyone else. Most of those guys had gone through similar problems to mine and were more than happy to provide guidance.

From the Kinesiology Department my gratitude has to be extended to Noriaki Okita, who was agreat source of help. Even though the work on hardware and network connections we have done is not complete, and thus will not be detailed in this thesis, he was important to the completion of my degree none-the-less. He is the expert of the motion capture lab, and I thank him for letting someone from the Aerospace Engineering Department come up and take over the lab.

Also I would like to thank the support system outside of Penn State. First that includes my family and friends. My father always cultivated a sense of wonder in the world around me. He created the nerd I am today and that is a great thing. He supported me, encouraged me to reach for this degree, and has always been there my whole life. My sister has always been there to talk to and even pretended to understand what I am talking about when she asks how things are. My grandparents and rest of the extended family also deserve recognition for encouraging

me to keep on striving for me to do my best. My thanks to all my friends for keeping me sane during my 6 years of college and happy enough to want to keep on pursuing this degree.

Included with my family and friends, because to me she is both, I would like to thank my supportive girlfriend of nearly 4 years Jacqueline. I talked to her more than anyone during my time as a graduate student, and she dealt with me every time I was stressed, tired, happy, sad, or otherwise. She knows more than anyone else how hard I have worked for this degree and has been my first supporter since we started dating.

Dedication

This is for my father. He was the largest influence in my life. Without him I don't know where I would be, what I would be doing or if I would enjoy it. I owe everything I have to him. Thank you so much Dad. I love you.

Dedication

Chapter 1

Introduction

This thesis presents a comprehensive solution for autonomously estimating the state of a moving platform via bearing measurements. The system is contained entirely onboard an unmanned aerial vehicle (UAV), and uses only information obtained via a visual camera system aided by a global positioning system and internal navigation system (GPS/INS), as well as an inertial measurement unit (IMU). The research performed was motivated by the problem of smaller UAVS having limited capability in naval operations. This is due to the fact that landing on a platform at sea can cause problems for even seasoned pilots (see Figure 1.1), much less the limited navigation systems onboard the UAVS discussed here. Small UAVS have payload restrictions far beyond that of larger counterparts, and require creative solutions in order to accomplish complex goals like those set out in this thesis.

Attempting to land on a moving landing platform will require the following abilities:

- To sense where landmarks are on the deck
- Perceive their position in a visual frame
- Estimate the deck state from those measurements
- Plan a path to land at some future time
- Possess the ability to control the aircraft in following that planned path

This thesis focuses on estimating the deck state using an integrated visual camera and landmarks on some given platform. The helicopter state is assumed to be provided by an onboard GPS/INS and IMU. Using these two measurement systems, an estimator, trajectory planner, and flight controller can be used to safely land on a platform for a variety of conditions.

Figure 1.1. An example of a manned helicopter landing on a ship deck subject to significant wave motion.
(http://www.youtube.com/watch?v=bC2XIGMI2kM)

However, this system faces multiple complications inherent to this problem. First, using only vision measurements can prove to contain some difficulties for estimating deck states. The measurement for each landmark being tracked on the deck is limited to bearings instead of physical positions. These nonlinear measurements must then be converted in order to find deck states. Also the Equations of Motion (EOMs) governing the estimation are not known by the estimator. The differences between the true kinematics and the estimated kinematics used by the estimator can lead to unmodeled dynamics within the system. This can create uncertainty or drift in the estimation and therefore can increase the odds for failure when a vehicle is attempting a landing. These discrepancies in estimation cannot be solved using simple, standard techniques, but by specific techniques formulated for this type of problem.

This thesis will serve the following functions:

- To depict a viable system for the deck and UAV state estimation involved in landing on a moving platform using only a monocular vision system and IMU contributions.
- To demonstrate that the estimation problems involved with this research can be solved by utilizing an Unscented Kalman Filter (UKF).
- Present results that establish the viability, accuracy, and reliability of the estimator via computer simulation

1.1 Motivation

The use of autonomous vehicles has the potential to change the world in both the commercial and military sectors. Unmanned aerial vehicles, particularly smaller models, do face more challenges than a piloted or larger vehicle including; the increased significance of external forces and disturbances, smaller payload capacity, and also the limited ability to carry as much sensing equipment as their larger counterparts. However, these vehicles are preferable to larger UAVS and piloted vehicles because of the decreased cost, and versatility to be employed for a wide variety of mission types.

Operating aircraft at sea adds a level of difficulty to landing or performing precise maneuvers coordinated with other vehicles, whether there is autonomy involved or not. Not only are the aircraft subject to the normal environmental forces, but the deck is now under the influence of the semi-random motion of waves, as well as natural phenomena such as currents and tides. In order to safely attempt a landing, these motions must be estimated to a high degree of accuracy, so that the UAV does not potentially crash or miss the target due to unforeseen external influences. In the case of non-specialized ships, where there is little to no communication between the ship and the helicopter, all sensors, computational ability, and controlling equipment must be kept onboard. This ensures the helicopter will always be able to provide itself with the information needed in order to safely land or maneuver relative to the deck.

While there is current capability to autonomously land on moving ship platforms, there are many restrictions. Only larger UAVS, with many sensors, in very calm seas, with a cooperative ship moving in a simple one directional fashion can accomplish such a task with consistency. However, even with the successes in the autonomous landing field to date, the scope of operations is relatively narrow compared to the goals of this research. Ultimately, this thesis seeks to enable landing on vessels ranging from frigates (Figure 1.2(a)), to multipurpose amphibious assault ships (Figure 1.2(b)), to naval capable hovercraft (Figure 1.2(c)), and on to riverine capable craft (Figure 1.2(d)).

This thesis describes a system that uses a monocular vision system, GPS/INS, and an inertial measurement unit to estimate the state (position, orientation, velocity, angular rate) of a ship deck to a sufficient accuracy where landing can be performed.

IMUs are commercially available and have a history of being used for vehicle state determination. Small, low powered IMUs are ideal for small UAV applications. However, IMUs are not a total solution to this thesis's navigation problem. They do not provide information about the deck state, only the vehicle states. Also IMUs are susceptible to noise and bias, which if left unchecked could lead to significant drift in measurements of some or all of the vehicle states. In order to solve the problem of drift, another measurement system must be utilized. For this research, intermittent GPS measurements onboard the vehicle, provide the correction necessary to deal with this drift issue. The camera must be utilized as the only system capable of measuring information about deck states.

Research has shown that monocular cameras are capable of being used for attitude or relative position measurements [34, 35, 16]. As camera technology has improved, so has their functionality with respect to measuring information about landmarks. By using prior knowledge about the landmarks in the camera frame, and previous frames, knowledge can be gained about deck position, attitude, velocity, and angular rate. Using multiple bearing measurements allows for an ever-improving estimate of the decks' state as well.

A schematic of the problem is shown in Figure 1.3.

(a)

(b)

(c)

(d)

Figure 1.2. An example of autonomous ship-board landing and the vessels targeted by this research

(a): A MQ-8B Fire Scout performing landing tests in 2009 (http://www.navair.navy.mil). (b): The USS Wasp on surge deployment (http://commons.wikimedia.org). (c): A Navy LCAC unit performing operations at sea http://commons.wikimedia.org). (d):A Riverine squadron 2 patrolling off Iraq in December 2007 (http://commons.wikimedia.org)

1.2 Framework for Vision-Based Landing

Autonomous landing on a ship deck is an extremely challenging objective. In order to successfully accomplish the goal of touching down safely; there are certain conditions that any system must be able to meet. The tasks this system must be able to perform are:

1. The UAV must be able to maintain controlled flight with the goal of being able to observe deck motion. This requires the vehicle to observe for long

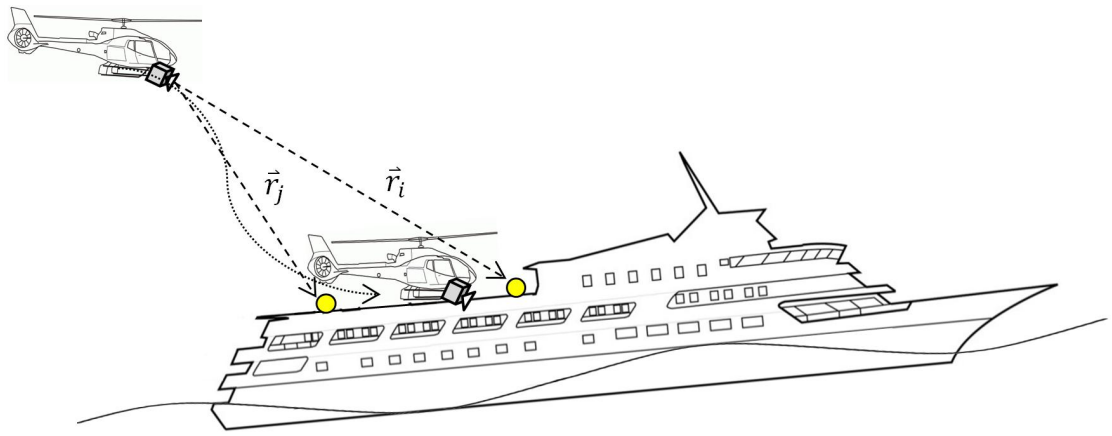

Figure 1.3. Two-Dimensional schematic depicting the autonomous ship-board landing problem.

enough, and provide observational diversity in order to accurately estimate deck state.

2. The UAV must be able to determine a goal position, as well as plan the best trajectory to said point on the deck. This trajectory can be planned to maximize measured information (the equivalent of minimizing covariance), or by planning the safest trajectory based on any one of a number of criteria.

3. Finally the UAV must be able to repeat these tasks as necessary given ambient conditions, unknown deck motion, and other possible causes in the deviation of the estimate. The vehicle must be able to recognize when its estimate is no longer accurate enough to use, and be able to return to a controlled observation status until a better estimate is tabulated. This fidelity monitoring is essential to any robust system, especially when there is a chance for significant monetary loss or loss of life.

For a full scale UAV to complete these tasks would be a challenge, but attempting them with a much smaller vehicle only exacerbates potential issues. The payload limitations of small UAVS means that there is less of a full sensor suite than what other vehicles might be equipped with. While GPS sensors are typically small, and are expected to be included onboard the vehicle; camera equipment and communication systems could potentially be restricted by these limitations. Also,

since there is little or no communication between the ship and the UAV there is little to no a priori knowledge of the ship deck motion or other state information. All that is measured about the deck are bearings in the camera frame; which are then used to produce relative deck states that are dependent on the UAV states.

The task of observational flight can be accomplished by taking a preplanned path towards the deck. Monitoring of the covariance estimates can be done, and adjustments to the approach and observation path can be made as needed in order maximize information. The approach does not have to be a straight line or any simple shape, something such as slalom curve or even a full circling of the deck may be the best observation approach. This observation method must also account for possible loss of observable markers due to occlusion or limitations of the camera's field of view.

Once the observation of the deck is performed and the estimated state covariance is satisfactory, a trajectory can be found for landing. Once the trajectory is found, a controller then forces the UAV out of observation mode and into a flight condition such that it can follow the planned trajectory as closely as possible while maintaining stability. This trajectory will need to be updated as the deck estimate is changing and the vehicle is approaching. The UAV must also be able to recognize if the deck state covariance is too large, indicating that the deck state estimate is too uncertain for safe landing. If something does go awry, the UAV could re-enter observation mode until confidence in deck state estimates is restored.

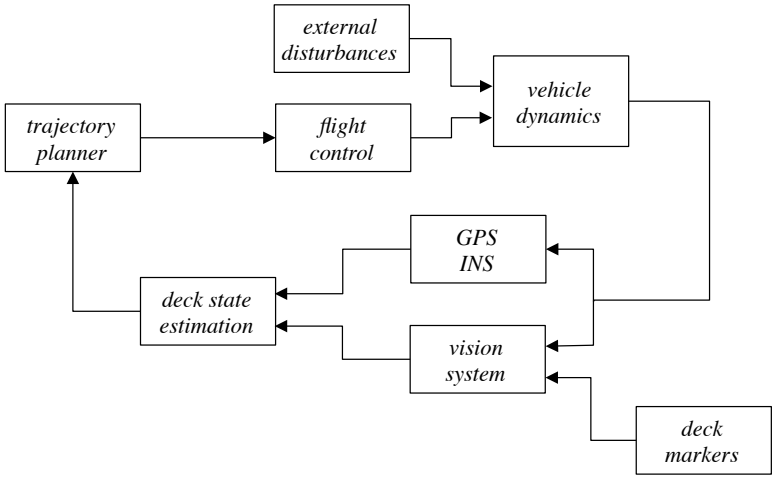

Figure 1.4. A top-level block diagram of an entire autonomous landing system

The top-level block diagram in Figure 1.4 depicts a system which would enable the vehicle to complete all the tasks detailed above. The framework begins with a trajectory planner and controller. Depending on whether the vehicle is in observation or landing path planning mode, the planner appropriately sets conditions for the vehicle to meet (i.e. maintain position behind deck, descend towards deck at 1 m/s). The flight controller then adjusts vehicle states such that the flight conditions match the path planning conditions as close as possible. The controller uses measurements of vehicle angular rates as well as accelerations in order to adjust those flight conditions. Finally, measurements of the deck are obtained via the on-board camera. Using the previously found vehicle state and the incoming camera measurement, an estimate of deck state is found which can be used to update the trajectory planner if necessary.

1.3 Estimator Overview

The defining piece of the system discussed in this thesis is the estimator that is able to take UAV states and vision measurements, and process them to determine estimates of the deck states. This estimator deals with an extremely nonlinear situation. Both deck motion and available measurements (azimuth and elevation to markers on the deck) are nonlinear. Furthermore, deck motion is difficult to predict accurately since it is driven by wave motion. Therefore, any deck state estimator must be able to handle significant nonlinearities in measurements and uncertainty in deck motion.

The main contribution of this thesis is a deck state estimation system that uses only sensing available on the helicopter. This on-board sensing consists of a GPS receiver, an inertial measurement unit, and a vision system. It is assumed that the vision system is able to compute bearings (azimuth and elevation) to features on the ship deck. In this thesis it is assumed that these features are fiducial markers, but a slightly more general approach (such as tracking corners) can also be used. It is not assumed that the markers are individually identifiable: thus the problem of data association is addressed in this thesis. To ensure that the system is general across a wide range of ship types, a specific ship model is not assumed. Rather, a second order kinematic model for ship deck motion is used. This model has the

advantage of simplicity and broad applicability, but at a cost of potentially reduced accuracy.

1.3.1 Data Association

When utilizing a Kalman filter, data association is of utmost importance. Without knowledge of which measurement corresponds to which target, the UKF is prone to divergence. The data association problem essentially consists of associating bearing measurements

$$\mathbf{z} = \begin{bmatrix} \gamma_{x1} & \gamma_{y1} & \gamma_{x2} & \gamma_{y2} & \cdots & \gamma_{xn} & \gamma_{yn} \end{bmatrix}$$

to targets $\begin{bmatrix} L_1 & L_2 & \cdots & L_n \end{bmatrix}$.

One solution to this problem is to design visually unique and identifiable targets. For this problem it could be done by coloring the landmarks or arranging them in a nonsymmetrical pattern that could be discerned by classical feature extraction techniques. However, an overarching theme of this research assumes that the targets are not unique. Thus, simply stating that the markers are inherently easy to differentiate is not an option.

By whatever means the data association is accomplished, it is imperative that the system be robust due to possible interference. This may be due to markers being occluded on the deck, markers leaving the camera's field of view during normal operations, or possibly losses of an entire measurement cycle. It is also important that the system remain operable when the targets have a high uncertainty in position, such as when the observation first starts.

In Section 3.2 this thesis presents a solution for the data association problem. The bearing measurements are compared from frame to frame, and once the bearings are found a variation of Munkres algorithm is used to determine the most accurate association.

1.3.2 Target Initialization

Any Kalman Filter needs a reasonable initial guess of all the states being estimated in order to work properly. If the initialization is too poor, then estimator divergence

or data association issues may arise. In this problem, it is assumed that the marker positions relative to the deck centroid are known in the decks' body coordinate frame. Therefore, by having accurate estimates of the deck's position and attitude, it is possible to estimate where one would expect the targets to appear in the camera frame at the initial time step.

1.4 Related Work

In recent years an immense amount of focus, funding, and work has been turned towards UAV operations. Some of the problems that the systems in this thesis will encounter (navigation, target tracking, motion estimation, etc.) have been analyzed to varying degrees, and within diverse frameworks of the scientific community. The following sections will attempt to segregate and analyze previous work into distinct categories.

1.4.1 Sea Related Operations and Wave Motion Modeling

Considerable work has been done previously in the field of sea related helicopter landing solutions. This work has included both manned and unmanned situations. For manned vehicles, work by Dr. Bernard de Ferrier has investigated the possibility of utilizing a Landing Period Designator to assist piloted landings [2]. This designator would attempt to determine, either in advance or at the current time, a period of low wave motion that is more conducive to attempting a landing. This designator was tested in manned simulators as a way to alert pilots when the best time to attempt a landing was with some success. In its current form the landing period designator requires a piloted vehicle. If this were to be outfitted for a UAV the landing period designator could potentially be used within a larger deck estimation system. The designator could provide a "go" or "no go" signal in conjunction with the deck state estimator.

Research with unmanned vehicles has studied the possibility of using a tether-based system for increasing sea-based landing viability. This would involve a UAV lowering a tether to an operator on the deck who would attach that line to the deck. Once attached, controllers were tested which utilize the property that the

tether can couple helicopter rotation and translation dynamics relative to the deck [21]. Essentially, the helicopter would be able to reel itself in, using the tether tension as a stabilizing force. While this solution is designed specifically for UAVS, it requires a human operator to physically attach and detach the tether. This can be difficult, dangerous, or downright impossible depending on the sea conditions.

A landing system that uses differential GPS, LIDAR and a vision system is described by Garratt et al. [6]. While successful, that system incorporates significant additional sensing, and only estimated a deck with fixed position.

While exact and specific models of ship motion in the presence of waves is not a focus of this research (indeed, the estimator makes no assumption of specific types of motion), this thesis does use a few motion models to assess the effect of unmodeled dynamics on deck state estimation. Both a stochastic wave model based on the Pierson-Moskowitz spectrum [22, 37] and a ship model based on a TMV 114 fast ferry [8] are used here.

1.4.2 Vision Based Navigation and State Estimation

The benefits of vision sensors on small UAVS has already been mentioned in this thesis, but much other research has come to the same conclusion. Many published documents have detailed potential usages for vision measurement systems in varied operational environments. Vision-based navigation for UAVS in applications such as flight control and relative navigation is discussed in [33, 38, 3, 11]

More closely related to the research in this thesis, using vision measurements for navigation in GPS denied and/or occluded environments has been reviewed [16, 15, 39, 35]. Also, more comprehensive, inertial guidance systems have been established [34, 35] which partially rely on vision measurements. More specific publications have also focused on: VTOL aircraft [13], increasing efficiency and safety for airfield operations [5], and integrated self-contained indoor navigation systems [7].

There have also been significant forays into utilizing vision systems for optimizing UAV state estimation in relation to trajectory determination. Specific publications detailing possible solutions to state estimation on small UAVS [36], with single vision sensors [33], and for low-resolution and/or quality imaging capability

[6].

With all of this work involving the usage of vision sensors within the scope of autonomous aircraft operations, several publications have discussed comprehensive solutions to the problem. These include research for using EKF techniques to estimate the same deck state vector used in this thesis [23]. However, this system was tested with a landing area that was not moving, simplifying aspects of the problem significantly. Two separate publications by Srikanth Saripalli and others have altered the scope to include moving targets [26, 27]. However, these works do not address the problem of estimating the state of a six degree of freedom deck.

In the scope of this thesis, vision systems are not being utilized just to navigate, but also to assist in knowledge of the environment around the UAV in relation to completing a given goal. In this case the vision subsystem is used to analyze deck motion, and eventually safely land upon the deck. This mission type contains several more general functions that research has shown vision systems are capable of performing.

Vision systems have been used for guidance and control of UAVS [12, 30]; landmark detection and mapping [15, 16, 29]; and obstacle avoidance [29, 32]. Further research has examined target tracking (including control) for single [9, 25] and multiple targets [17, 28]. A vision based landing system for a tailsitter is discussed in [18].

As stated earlier, data association is a critical part of the deck state estimation process. The Munkres algorithm was originally proposed as a means of optimally solving the task assignment problem [14], and has been used to solve the data association problem as well in the context of landmark tracking [10], feature mapping [24] and obstacle detection [1].

1.5 Summary of Contributions

- **Framework for Autonomous Ship-board Landing**
  A system that enables observation of ship deck motion; where all components are contained onboard a small UAV using measurements of a monocular camera, an IMU, and possibly occasional GPS measurements. The capabilities and limitations of this system and these measurement types will be evaluated.

- **Estimator Design**
  The development of a robust estimator that utilizes an Unscented Kalman Filter in order to estimate generic ship motion. Deck states (position, attitudes, velocities, angular rates), are estimated, while UAV states are assumed to be known. This information would be utilized by a trajectory planner in order to compute the optimal landing path.

- **Performance Verification: MATLAB Simulation**
  Monte Carlo results of simulations involving deck state estimation with a variety of sea states and wave modeling techniques prove that the system detailed in this thesis provides a generic solution to the landing problem independent of ship and specific wave motion There is a strong relationship between error and covariance; both decrease as the UAV approaches the deck, and acquires more measurements. Once the estimation is accurate enough, a trajectory planned can safely guide the helicopter to safe landing.

1.6 Reader's Guide

The remainder of the thesis is organized as follows:

Chapter 2: The Deck State Estimation Problem describes what information is necessary in order to solve the problem described in this thesis. Explanations of coordinate frames, deck kinematic model, vision measurement model, and ship deck motion models are all included. This is followed by a study of observability issues within the estimation problem. Finally an outline of the UKF used to estimate the system is introduced.

Chapter 3: Implementation Using a UKF further delves into the estimation problem and the challenges inherent to this application. A more detailed implementation of the UKF algorithm is presented, and definition of vision measurement noise and filter process noise is shown. This leads into an analysis of data association techniques. This chapter concludes with a brief outline of how deck estimate and associated covariance is initialized.

Chapter 4: Estimator Simulation Results presents both the representative run analysis and results of Monte Carlo simulations of estimation of deck state. This analysis is performed for all wave motion models discussed in Chapter 2. State estimates and uncertainty characteristics, as well as other trends are all analyzed in 3D space simulations. The results here prove that an effective, efficient, robust estimator has been developed.

Chapter 5: Conclusion summarizes the results of this research and provides potential areas of focus for future work.

Chapter 2

The Deck State Estimation Problem

This chapter fully details the estimation problem introduced in Chapter 1. It also serves the purpose of developing equations for the sensor measurements and kinematics of all involved systems. This chapter ends at dynamics development; however, the implementation and results are discussed in following chapters. This includes how all these dynamics are executed in a real-time simulation within the UKF.

Section 2.1 describes the estimation problem and state variables involved. Section 2.2 details models for deck kinematics, vision sensors, and various wave motions. Section 2.3 discusses the issue of estimating unobservable wave states, which motivated the current design of the estimator that is used in this thesis. Section 2.4 provides an introduction to nonlinear estimation techniques such as the UKF, and outlines this recursive estimation process. To conclude, Section 2.5 contains a summary of all the modeling and kinematic information covered thus far.

2.1 Problem Statement

As outlined in Chapter 1, the scenario considered in this thesis involves an unmanned rotorcraft attempting to land on a ship deck which is being forced by unknown wave motion. The rotorcraft is equipped with a GPS/INS to compute vehicle states and a monocular camera for measuring relative deck states: only sensors available on the helicopter will be used for landing. A schematic of the estimation problem at hand is shown in Figure 2.1.

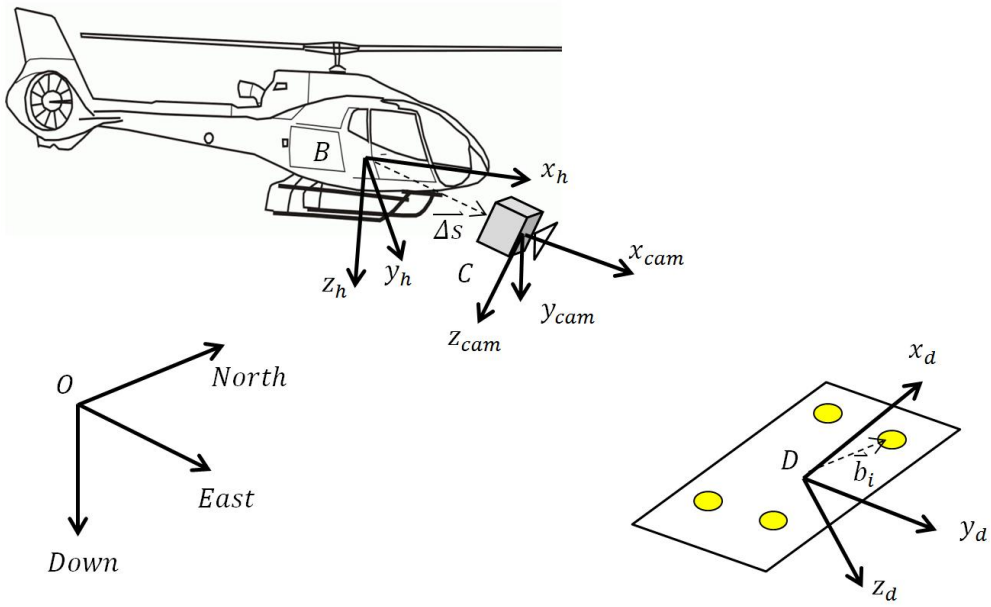

Figure 2.1. A schematic depicting the estimation problem at hand.
The aircraft obtains bearings to markers fixed to the deck and knowledge of its own state from INS/GPS. *Using these measurements an estimate of deck position, orientation, velocity and angular rate must be obtained.*

Notionally, the problem of landing is assumed to comprise two main phases: approach to a landing initiation point and landing. During the approach phase the vision system tracks features on the deck; the combination of measured bearings to these features and knowledge of helicopter state is used to compute an estimate of deck state and an associated covariance. The estimate of covariance can be used to determine if deck state has been determined with sufficient certainty to permit landing.

While the path flown during approach can have a significant impact on the accuracy of deck state estimation it is not the focus of this thesis.

Landing on the ship deck requires knowledge of deck position and orientation. Further, knowledge of deck velocity and angular rate is required to ensure that relative speed between the rotorcraft and the ship deck at touchdown is within acceptable limits. Thus the deck state vector is

$$\mathbf{x}_d = [x_d \; y_d \; z_d \; \phi_d \; \theta_d \; \psi_d \; u_d \; v_d \; w_d \; p_d \; q_d \; r_d]^T \tag{2.1}$$

Referring to Equation 2.1, the first three terms of the deck state vector represent position in a north-east-down (NED) inertial reference frame; the second three terms denote deck orientation with respect to the NED frame (as NASA-standard Euler angles); the next three terms represent deck velocity expressed in the inertial frame; and the last three terms denote angular rates about the deck body-fixed axes.

The helicopter state $\mathbf{x}_h$ (assumed known) is

$$\mathbf{x}_h = [x_h \; y_h \; z_h \; \phi_h \; \theta_h \; \psi_h \; u_h \; v_h \; w_h]^T \tag{2.2}$$

The first three terms denote position in the NED frame, the next three terms represent orientation with respect to the NED frame, and the last three terms denote velocity expressed in the vehicle's body frame. States are summarized in Table 2.1.

Table 2.1. State Information and Determinations

State	Usage	Determined By
Deck Positions	Landing Controller	Estimator
Deck Attitudes	Landing Controller	Estimator
Deck Velocities	Landing Controller	Estimator
Deck Angular Rates	Landing Controller	Estimator
Vehicle Positions	Observation/Navigation	known via GPS/INS
Vehicle Attitudes	Observation/Navigation	known via GPS/INS
Vehicle Velocities	Observation/Navigation	known via GPS/INS

Given the limited sensing available and the unknown wave states driving ship deck motion, the problem at hand is to obtain enough information about the deck state to permit a safe landing. That is, the problem is to compute an estimate $\hat{\mathbf{x}}_d$ and associated covariance $\mathbf{P}$ of the deck state $\mathbf{x}_d$ using a process model

$$\dot{\mathbf{x}}_d = f(\mathbf{x}_d, \mathbf{u}) \tag{2.3}$$

and measurement model

$$\mathbf{z} = g(\mathbf{x}_h, \mathbf{x}_d) \tag{2.4}$$

Here $\mathbf{u}$ represents inputs and disturbances to the ship deck and $\mathbf{z}$ represents measurements from the vision system sensors. The deck motion model is described in Section 2.2.2 and the vision measurement model is described in Section 2.2.3.

Chapter 3 describes the implementation of these system models into the prediction and correction steps of a nonlinear estimator.

2.2 System and Sensor Models

2.2.1 Coordinate Frames

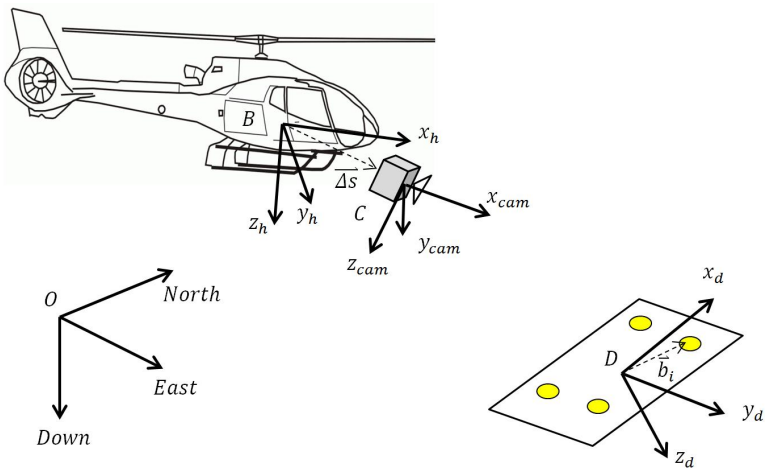

Figure 2.2. Definition of Relevant Coordinate Frames

All reference and coordinate frames defined in this section are depicted in Figure 2.2. The inertial frame for this problem is a standard North-East-Down (NED) coordinate frame. This frame, centered on point O, is used for the global navigation of the UAV. Since the time required for landing and the distance flown during landing is typically short, this flat Earth model is adequate for navigation.

Sensors (i.e. the camera and GPS/INS) are fixed in the vehicle's body frame B. It is assumed that the camera is located at a known (stationary) point in the vehicle body frame and the orientation of the camera with respect to the body frame is constant and known. Bearings to deck markers are obtained in the camera frame C. Transformation matrices $\mathbf{T}$ and $\mathbf{T}_{cam}$ define the transformation of a vector in O to B and from B to C, respectively. Finally a deck frame D is fixed to the ship deck, and a transformation matrix $\mathbf{T}_d$ defines the transformation of a vector in O to D.

The transformation matrix is defined by Euler angles of one frame with respect to another. This matrix is used to convert from the NED to deck body frame. Following the NASA standard roll-pitch-yaw convention,

$$\mathbf{T} = \mathbf{T}_\phi \mathbf{T}_\theta \mathbf{T}_\psi \tag{2.5}$$

with

$$\mathbf{T}_\phi = \begin{bmatrix} 1 & 0 & 0 \\ 0 & \cos\phi & \sin\phi \\ 0 & -\sin\phi & \cos\phi \end{bmatrix} \tag{2.6}$$

$$\mathbf{T}_\theta = \begin{bmatrix} \cos\theta & 0 & -\sin\theta \\ 0 & 1 & 0 \\ \sin\theta & 0 & \cos\theta \end{bmatrix} \tag{2.7}$$

$$\mathbf{T}_\psi = \begin{bmatrix} \cos\psi & \sin\psi & 0 \\ -\sin\psi & \cos\psi & 0 \\ 0 & 0 & 1 \end{bmatrix} \tag{2.8}$$

Thus

$$\mathbf{T} = \begin{bmatrix} \cos\theta\cos\psi & \cos\theta\sin\psi & -\sin\theta \\ \sin\phi\sin\theta\cos\psi - \cos\phi\sin\psi & \sin\phi\sin\theta\sin\psi + \cos\phi\cos\psi & \sin\phi\cos\theta \\ \cos\phi\sin\theta\cos\psi + \sin\phi\sin\psi & \cos\phi\sin\theta\sin\psi - \sin\phi\cos\psi & \cos\phi\cos\theta \end{bmatrix} \tag{2.9}$$

2.2.2 Deck Kinematic Model

To keep the deck motion model general across a wide variety of ships and boats a second order kinematic model driven by Gaussian noise is used. This is a constant acceleration model, and clearly there will be significant unmodeled dynamics (acceleration of a ship deck driven by wave motion is not constant!). However, the simplicity and broad applicability of this model makes it an attractive choice.

Both deck position and velocity are expressed in the inertial frame, so that

$$\dot{x}_d \;=\; u_d \tag{2.10}$$

$$\dot{y}_d = v_d \tag{2.11}$$
$$\dot{z}_d = w_d \tag{2.12}$$

Body angular rates can be expressed as Euler angle rates by

$$\dot{\phi}_d = p_d + q_d \sin\phi_d \tan\theta_d + r_d \cos\phi_d \tan\theta_d \tag{2.13}$$
$$\dot{\theta}_d = q_d \cos\phi_d - r_d \sin\phi_d \tag{2.14}$$
$$\dot{\psi}_d = q_d \frac{\sin\phi_d}{\cos\theta_d} + r_d \frac{\cos\phi_d}{\cos\theta_d} \tag{2.15}$$

Deck acceleration and angular acceleration are driven by unknown forcing functions

$$\dot{u}_d = F_{d_u} \tag{2.16}$$
$$\dot{v}_d = F_{d_v} \tag{2.17}$$
$$\dot{w}_d = F_{d_w} \tag{2.18}$$
$$\dot{p}_d = F_{d_p} \tag{2.19}$$
$$\dot{q}_d = F_{d_q} \tag{2.20}$$
$$\dot{r}_d = F_{d_r} \tag{2.21}$$

Ultimately, deck motion is forced by waves acting upon the ship. To avoid a specific ship model, here the forcing term

$$\mathbf{F}_d = \begin{bmatrix} F_{d_u} & F_{d_v} & F_{d_w} & F_{d_p} & F_{d_q} & F_{d_r} \end{bmatrix}^T \tag{2.22}$$

is assumed be zero-mean Gaussian random noise:

$$\mathbf{F}_d \sim \mathcal{N}(0, \mathbf{Q}) \tag{2.23}$$

The covariance $\mathbf{Q}$ of this forcing term must be large enough to "cover" the unmodeled dynamics. It will be determined based on sea state. The actual value of the covariance of $\mathbf{Q}$ will be defined in Section 3.1.1.

2.2.3 Vision Model

The camera is located at a known position $\Delta\mathbf{s}$ from the helicopter center of gravity with a known rotation $\mathbf{T}_{cam}$ with respect to the vehicle body frame. The camera's x-axis is the optical axis, so that camera y and z axes lie in the image plane.

For a vector $\mathbf{s}$ expressed in the camera frame, the pinhole projection model defines that vector's projection onto the image plane:

$$\mathbf{z} = \frac{f}{s_x} \begin{bmatrix} s_y \\ s_z \end{bmatrix} \tag{2.24}$$

where f is the focal length and s_x, s_y, and s_z denote the components of the vector expressed in the camera frame.

The pinhole projection model becomes ill conditioned for vectors that are nearly perpendicular to the optical axis. A modified pinhole model computes bearings (azimuth and depression angle: here a positive angle is down with respect to the camera's optical axis) as the arctangent of the pinhole projection. A comparison of the two vision models is shown in Figure 2.3 [16]. For the i^{th} deck marker the vision model g_i is

$$\mathbf{z}_i = \begin{bmatrix} \arctan\left(\frac{s_{i,y}}{s_{i,x}}\right) \\ \arctan\left(\frac{s_{i,z}}{s_{i,x}}\right) \end{bmatrix} + \mathbf{n}_c \tag{2.25}$$

The measurement is corrupted by zero-mean Gaussian random noise $\mathbf{n}_c$. The vector $\mathbf{s}_i$ represents the vector to the i^{th} marker, expressed in the camera frame:

$$\mathbf{s}_i = \mathbf{T}_{cam} \left[\mathbf{T} \begin{bmatrix} x_i - x_h \\ y_i - y_h \\ z_i - z_h \end{bmatrix} - \Delta s \right] \tag{2.26}$$

where $\mathbf{x}_i = [x_i \; y_i \; z_i]^T$ is the position of the i^{th} marker in the inertial frame.

The position of a deck marker in the inertial frame is dependent on the deck

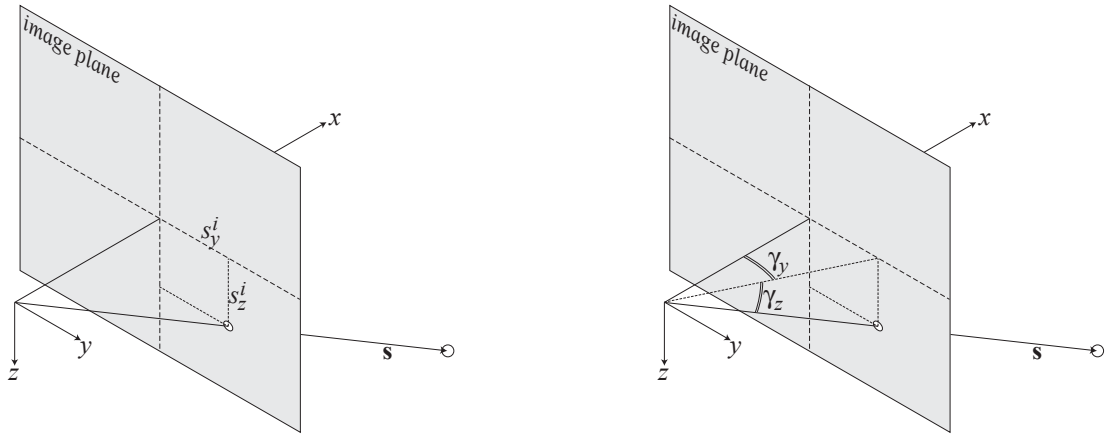

(a) Pinhole model.

(b) Modified pinhole model.

Figure 2.3. Comparison of vision models.

position, deck orientation and the position of the marker in the deck frame:

$$\mathbf{x}_i = \begin{bmatrix} x_d \\ y_d \\ z_d \end{bmatrix} + \mathbf{T}_d^{-1}\mathbf{b}_i \tag{2.27}$$

where $\mathbf{b}_i$ is the location of the i^{th} marker in the deck frame (assumed known).

2.2.4 Modeling Ship Deck Motion

Ship deck motion can be very complex: in essence it is the dynamics of the ship driven by wave motion. Ship motion modeling is not the focus of this thesis, but a brief discussion is warranted to give confidence in the deck state estimation results.

2.2.4.1 Sinusoidal Method

The simplest model of deck motion is independent sinusoidal forcing of each degree of freedom. In this model each degree of freedom is driven by

$$F_{d_{(\cdot)}}(t) = -A_{(\cdot)}\omega_{(\cdot)}^2 \sin\left(\omega_{(\cdot)}t + \varphi_{(\cdot)}\right) \tag{2.28}$$

Here A is the wave amplitude, ω is the frequency, and φ is phase. $(\cdot)$ denotes a particular degree of freedom (x, y, z, ϕ, θ, ψ).

Integrating this forcing term twice gives simple sinusoidal motion for each degree of freedom with amplitude A, frequency ω and phase φ. Note that amplitude, frequency, and phase can be specified independently for each degree of freedom.

2.2.4.2 Stochastic Method

While the sinusoidal model gives motion that "looks" realistic, in practice that model gives very regular motion. True ship motion is far less regular, with significant changes in motion amplitude from one wave to the next.

To model this more complex motion a sum-of-sinusoids is used, so that [22]:

$$F_{d_{(\cdot)}}(t) = \sum_{k=1}^{N} -A_{(\cdot),k}\omega_{(\cdot),k}^2 \sin\left(\omega_{(\cdot),k}t + \varphi_{(\cdot),k}\right) \tag{2.29}$$

Choosing random, uniformly distributed values of $\varphi_{(\cdot),k}$ will give a wave shape that appears random. The problem now is making an appropriate choice of amplitudes $A_{(\cdot),k}$ and frequencies $\omega_{(\cdot),k}$: these can be computed after a particular wave power spectrum has been defined.

The Pierson-Moskowitz spectrum [37] is an empirically derived power spectrum that defines wave energy as a function of frequency for a fully developed sea. The power spectral density is

$$S_{PM}(\omega) = \frac{0.78}{\omega^5}\exp(\frac{-3.11}{\omega^4 h_{1/3}^2}) \tag{2.30}$$

Here $h_{1/3}$ is the mean wave height, which is defined based on sea state. The frequency for peak power density is

$$\omega_0 = 1.26 h_{1/3}^{-0.5} \tag{2.31}$$

Sea state is a numerical designation ranging from 0 (glassy calm) to 9 (wave heights exceed fourteen meters) that defines wave height. Table 2.2 gives parameters for sea states 1, 5, and 7; Figure 2.4 shows the Pierson-Moskowitz amplitude spectrum for those sea states.

Table 2.2. Sea state, mean wind speed and Pierson-Moskowitz parameters

Seastate	Approx. Windspeed (kt)	Vertical Wave Height (m)	Average Wave Period (s)	Range of Periods (s)
1	7	1	2	1-3.5
5	23	2.5	6	3.5-11
7	43	6.5	12	6.5-21

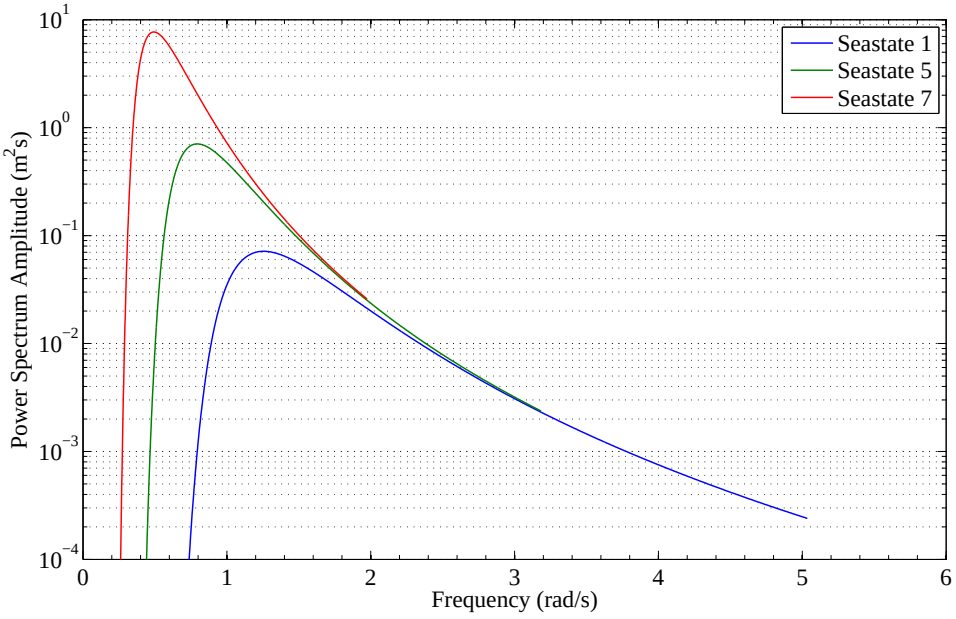

Figure 2.4. Pierson-Moskowitz amplitude spectrum for Sea State 1, 5, and 7

To represent a wave condition that has the Pierson-Moskowitz spectral density, amplitudes for a set of frequencies ω_k and associated bandwidths $\Delta\omega_k$ are computed as

$$A_k = \sqrt{2S_{PM}(\omega_k)\Delta\omega_k} \tag{2.32}$$

Now an appropriate range of frequencies must be selected. Figure 2.4 shows that wave amplitude is near zero for frequencies less than one quarter the peak frequency and greater than 4 times the peak frequency. To obtain good resolution over this frequency range, one-third octave bands in the range $\left[\frac{\omega_0}{4},\ 4\omega_0\right]$ are used. Band frequency limits and bandwidth are given in Table 2.3.

Figure 2.5 shows a wave for sea state 5 generated using this approach.

Table 2.3. One-third octave band frequencies in terms of ω_0

Center	Lower	Upper	Bandwidth
$0.25\omega_0$	$0.2227\omega_0$	$0.2806\omega_0$	$0.0579\omega_0$
$0.315\omega_0$	$0.2806\omega_0$	$0.3536\omega_0$	$0.0729\omega_0$
$0.397\omega_0$	$0.3536\omega_0$	$0.4455\omega_0$	$0.0919\omega_0$
$0.5\omega_0$	$0.4455\omega_0$	$0.5612\omega_0$	$0.1158\omega_0$
$0.63\omega_0$	$0.5612\omega_0$	$0.7071\omega_0$	$0.1459\omega_0$
$0.794\omega_0$	$0.7071\omega_0$	$0.8909\omega_0$	$0.1838\omega_0$
ω_0	$0.8909\omega_0$	$1.123\omega_0$	$0.2316\omega_0$
$1.26\omega_0$	$1.123\omega_0$	$1.414\omega_0$	$0.2918\omega_0$
$1.587\omega_0$	$1.414\omega_0$	$1.782\omega_0$	$0.3676\omega_0$
$2\omega_0$	$1.782\omega_0$	$2.245\omega_0$	$0.4631\omega_0$
$2.52\omega_0$	$2.245\omega_0$	$2.828\omega_0$	$0.5835\omega_0$
$3.175\omega_0$	$2.828\omega_0$	$3.564\omega_0$	$0.9263\omega_0$
$4\omega_0$	$3.564\omega_0$	$4.489\omega_0$	$1.167\omega_0$

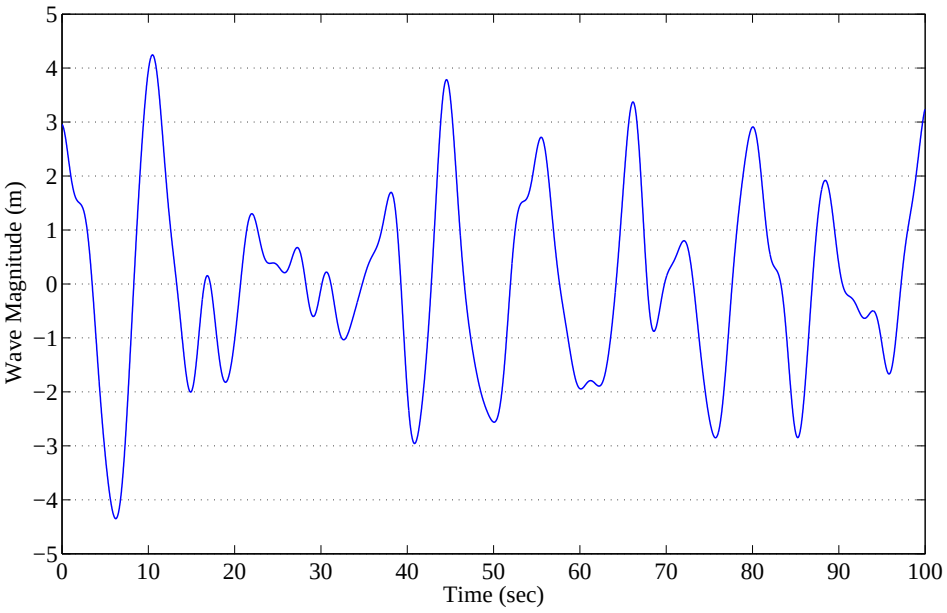

Figure 2.5. Sample wave generated using the Pierson-Moskowitz spectrum at sea state 5

2.2.4.3 Fast Ferry Ship Model

Ship motion is wave motion modulated by ship dynamics. The two previous deck motion models do not include ship dynamics, thus a model of direct ship motion

is useful to more accurately assess estimator performance.

In [8] Hess defines a motion model for a TMV 114 fast ferry. This ship is 113.5m in length, has beam 16.5m and displacement 700 metric tonnes (Figure 2.6).

Figure 2.6. A pictoral representation of the ferry used to accumulate data for this wave motion model.

(http://www.rodriquez.it)

Hess defines the EOMs for the ferry as:

$$y = 6.6 \sin \phi \tag{2.33}$$

$$z = 57.11 \sin \theta + 13.2 \sin^2 0.5\phi + 0.2172 \sin 0.4t \tag{2.34}$$
$$+0.4174 \sin 0.5t + 0.3592 \sin 0.6t + 0.2227 \sin 0.7t$$

$$\phi = 0.021 \sin 0.46t + 0.0431 \sin 0.54t \tag{2.35}$$
$$+0.290 \sin 0.62t + 0.022 \sin 0.67t$$

$$\theta = 0.005 \sin 0.46t + 0.00964 \sin 0.58t \tag{2.36}$$
$$+0.00725 \sin 0.7t + 0.00845 \sin 0.82t$$

The x position, and yaw angle are not as simply defined. For this research, x position and yaw angle wave forces were left to be determined by the stochastic model, while the other four wave forces use this fast ferry ship model. It is important to note that this motion model is only defined for "moderate wave motion" (sea state 4).

2.3 Wave State Estimation and Observability Issues

In principle the problem of landing would be made significantly easier if one could predict the deck state at some time in the future. For this to be possible in the estimation process proposed here the wave states would have to be defined and estimated. To examine the feasibility of this approach, consider a one degree of freedom ship deck (constrained to move only in the vertical direction), forced by simple sinusoidal motion.

For this single degree of freedom ship deck the states to be estimated are

$$\mathbf{x} = [z \ w \ A \ \omega]^T \tag{2.37}$$

where z is deck height, w is deck vertical velocity, A is wave amplitude and ω is wave frequency.

Assuming that wave amplitude and frequency are constant,

$$\dot{z} = w \tag{2.38}$$
$$\dot{w} = -A\omega^2 \sin \omega t \tag{2.39}$$
$$\dot{A} = 0 \tag{2.40}$$
$$\dot{\omega} = 0 \tag{2.41}$$

Where A is the amplitude of the wave and ω is the wave frequency. Written compactly,

$$\dot{\mathbf{x}} = f(\mathbf{x}) \tag{2.42}$$

Now suppose that only a measurement of deck height z is available:

$$y = [1 \ 0 \ 0 \ 0] \, \mathbf{x} = \mathbf{C}\mathbf{x} \tag{2.43}$$

An analysis of observability will reveal if it is possible to estimate wave states directly given measurements of deck position. Linearizing the equations of motion:

$$\delta\dot{\mathbf{x}} = \mathbf{A}\delta\mathbf{x} \tag{2.44}$$

Here

$$\mathbf{A} = \nabla f = \begin{bmatrix} 0 & 1 & 0 & 0 \\ 0 & 0 & a & b \\ 0 & 0 & 0 & 0 \\ 0 & 0 & 0 & 0 \end{bmatrix} \tag{2.45}$$

with

$$a = -\omega^2 \sin \omega t \tag{2.46}$$

$$b = -2A\omega \sin \omega t - A\omega^2 \cos \omega t \tag{2.47}$$

Writing down the observability matrix for this four state system,

$$\mathbf{O} = \begin{bmatrix} \mathbf{C} \\ \mathbf{CA} \\ \mathbf{CA}^2 \\ \mathbf{CA}^3 \end{bmatrix} = \begin{bmatrix} 1 & 0 & 0 & 0 \\ 0 & 1 & 0 & 0 \\ 0 & 0 & a & b \\ 0 & 0 & 0 & 0 \end{bmatrix} \tag{2.48}$$

This is not full rank, thus it is not possible to directly estimate wave states with a measurement of only deck height. Even if a measurement of deck vertical velocity is included it is not possible to directly estimate wave states. While it may be possible to obtain an estimate of wave states using a sequence of measurements, but that is beyond the scope of this thesis.

2.4 Sigma Point Kalman Filters

Any non-specific recursive estimator generally has two main steps. First the estimator predicts the next state using the prescribed kinematics. This is followed by the estimator correcting that update using incoming measurements. Now it has already been discussed that both the kinematics and the measurement model being utilized are nonlinear, and that measurement is corrupted by inherent noise. This combination of nonlinearity and uncertainty in measurement can lead to complications where estimators relying on linear EOMs would fail. Thus it is imperative that an estimator that is capable of working in a nonlinear environment be employed.

It has been shown in [16] that the Sigma Point Kalman Filter, also known as

an Unscented Kalman Filter, is capable of such a task. This filter does not need to approximate EOMs in an attempt to linearize the system. Instead the UKF assumes a Gaussian probability distribution function of state variables. This distribution is represented by a set of sigma points, which are used to capture the mean of the covariance of each state in the state vector. The UKF algorithm is shown in Figure 2.7. Further implementation of this will be elaborated on in the following chapter.

2.5 Summary: The Estimation Problem

In order to successfully land on the ship's deck, the UAV must maintain controlled flight, successfully observe marker motion during controlled flight, estimate deck motion from these measurements, plan and constantly update a landing path, and successfully execute that landing path. The focus of this thesis is on observing markers and then using those bearing measurements to compute a deck state estimate. This requires knowledge of all the vehicle states (assumed) as well as prior estimates of all the deck states listed in Section 2.1.

It has been detailed that due to unmodeled dynamics associated with deck motion, filter process noise must be introduced to mitigate poor estimator knowledge of true deck dynamics. This provides a simplistic, but very general, kinematic model for the estimator to use when determining deck motion. This noise must be related to the strength of wave motion affecting the deck (i.e. Pierson-Moskowitz Spectrum).

All deck state estimates will be found via the vision measurement system. The modified pinhole model will be implemented as the vision measurement model.

Different modeling techniques for wave motion were introduced. These included the sinusoidal model, the stochastic model, and the fast ferry ship model.

Due to the wave motion and vision measurement model chosen, estimation must be performed with a recursive estimator capable of nonlinear estimation (such as a UKF). The recursive estimator will create an estimation of deck state as well as an associated covariance.

It is important to repeat here that since all measurement systems are internal to the vehicle, very little information is shared from the deck to the vehicle, and

initialize with $\hat{\mathbf{x}}_0$ and $\mathbf{P}_{0|0}$.

For t_k, $k \in (1, \ldots, \infty)$ compute sigma points:

$$\mathbf{X}_{k-1|k-1} = \left[\begin{array}{ccc} \hat{\mathbf{x}}_{k-1|k-1} & \hat{\mathbf{x}}_{k-1|k-1} + \eta\sqrt{\mathbf{P_{k-1|k-1}}} & \hat{\mathbf{x}}_{k-1|k-1} + \eta\sqrt{\mathbf{P_{k-1|k-1}}} \end{array} \right] \tag{2.49}$$

Time update (prediction):

$$\mathbf{X}_{k|k-1} = f(\mathbf{X}_{k-1|k-1}, \mathbf{u}_{k-1}) \tag{2.50}$$

$$\hat{\mathbf{x}}_{k|k-1} = \mathbf{X}_{k|k-1}\mathbf{w}_m \tag{2.51}$$

$$\mathbf{P}_{k|k-1} = \left[\mathbf{X}_{k|k-1} - \hat{\mathbf{x}}_{k|k-1}\mathbf{1}\right] \mathbf{W}_c \left[\mathbf{X}_{k|k-1} - \hat{\mathbf{x}}_{k|k-1}\mathbf{1}\right]^T + \mathbf{Q} \tag{2.52}$$

Measurement update (correction):

$$\mathbf{Z}_{k|k-1} = h(\mathbf{X}_{k|k-1}) \tag{2.53}$$

$$\hat{\mathbf{z}}_{k|k-1} = \mathbf{Z}_{k|k-1}\mathbf{w}_m \tag{2.54}$$

$$\mathbf{P}_{zz} = \left[\mathbf{Z}_{k|k-1} - \hat{\mathbf{z}}_{k|k-1}\mathbf{1}\right] \mathbf{W}_c \left[\mathbf{Z}_{k|k-1} - \hat{\mathbf{z}}_{k|k-1}\mathbf{1}\right]^T + \mathbf{R} \tag{2.55}$$

$$\mathbf{P}_{xz} = \left[\mathbf{X}_{k|k-1} - \hat{\mathbf{x}}_{k|k-1}\mathbf{1}\right] \mathbf{W}_c \left[\mathbf{Z}_{k|k-1} - \hat{\mathbf{z}}_{k|k-1}\mathbf{1}\right]^T \tag{2.56}$$

$$\mathbf{K} = \mathbf{P}_{xz}\mathbf{P}_{zz}^{-1} \tag{2.57}$$

$$\hat{\mathbf{x}}_{k|k} = \hat{\mathbf{x}}_{k|k-1} + \mathbf{K}(\mathbf{A}\mathbf{z}_k - \hat{\mathbf{z}}_{k|k-1}) \tag{2.58}$$

$$\mathbf{P}_{k|k} = \mathbf{P}_{k|k-1} - \mathbf{K}\mathbf{P}_{zz}\mathbf{K}^T \tag{2.59}$$

There are $2N+1$ sigma points, where N is the dimension of the state vector. In this algorithm η is a weight factor, $\mathbf{w}_m$ is a vector of weights, $\mathbf{W}_c$ is a diagonal matrix of weights, $\mathbf{1}$ is a $(1 \times 2N+1)$ matrix of ones, $\mathbf{Q}$ is process noise and $\mathbf{R}$ is measurement noise. The weight factors are calculated as

$$\eta = \alpha\sqrt{N} \tag{2.60}$$

The constant α is a parameter which determines the spread of the sigma points. Typically $10^{-4} \leq \alpha \leq 1$. The weight vector $\mathbf{w}_m$ and weight matrix $\mathbf{W}_c$ are

$$\mathbf{w}_{m,1} = \tfrac{\alpha^2-1}{\alpha^2} \qquad \mathbf{w}_{m,i} = \tfrac{1}{2N\alpha^2} \tag{2.61}$$

$$\mathbf{W}_{c,1} = \tfrac{\alpha^2-1}{\alpha^2} + (1 - \alpha^2 + \beta) \qquad \mathbf{W}_{m,ii} = \tfrac{1}{2N\alpha^2} \tag{2.62}$$

where $i = 2, \ldots, (2N+1)$. The parameter β incorporates prior knowledge of the distribution of the state vector. For Gaussian distributions $\beta = 2$ is optimal [31].

Figure 2.7. Algorithm for Unscented Kalman Filter.
reproduced from Rudolph van der Merwe and Eric Wan, [31]

the estimated deck model has no resemblance to the true model; this system could potentially be implemented in many other situations: Underwater vehicles, ground vehicles, space system rendezvous, and innumerable others.

An implementation of the UKF is given in the following chapter, and computer simulation results are detailed in Chapter 4.

Chapter 3

Implementation Using a UKF

While the EOMs defining true deck motion are detailed in Section 2.2.2, and the vision measurement model was discussed in Section 2.2.3; These independent systems of equations must be implemented in an estimator in order to generate the a current best deck state estimate $\hat{\mathbf{x}}_d$. The UKF follows a specific algorithm wherein a set of sigma (test) points around the previous time steps best estimate are found. Those test points are then used to find the set of current estimated states with the lowest possible covariance. Once those new states are found, the state vector is updated as well as the covariance matrix.

While the algorithm was introduced in Figure 2.7, the steps being taken and definition of key components of the estimator is performed here. Lengthier discussions into the merits of the UKF over other estimators (such as the EKF) are contained in [16, 15, 31].

3.1 Deck State Estimation

As stated in Chapter 2 the state vector to be estimated is

$$\mathbf{x}_d = [x_d \; y_d \; z_d \; \phi_d \; \theta_d \; \psi_d \; u_d \; v_d \; w_d \; p_d \; q_d \; r_d]^T \tag{3.1}$$

Both the process model

$$\dot{\mathbf{x}}_d = f(\mathbf{x}_d, \mathbf{F}_d) \tag{3.2}$$

and measurement model

$$\mathbf{z} = g(\mathbf{x}_d, \mathbf{x}_h) + \mathbf{n}_c \tag{3.3}$$

were developed in Chapter 2.

The Unscented Kalman Filter follows a recursive process of prediction followed by correction. Here the prediction step is driven by the deck kinematic model and unknown process noise, and a key parameter is the magnitude of process noise that should be incorporated into the estimator. In this thesis process noise is computed based on the maximum expected acceleration of the deck. The correction step is driven by bearing measurements to deck markers combined with knowledge of helicopter position and orientation.

3.1.1 Prediction Step

The deck kinematics developed from Equation 2.10 to Equation 2.21 can be written compactly as

$$\dot{\mathbf{x}}_d = f(\mathbf{x}_d) + \begin{bmatrix} \mathbf{0}_6 \\ \mathbf{I}_6 \end{bmatrix} \mathbf{F}_d \tag{3.4}$$

where $\mathbf{0}_6$ is a 6×6 matrix of zeros, $\mathbf{I}_6$ is a 6×6 identity matrix, and $\mathbf{F}_d \sim \mathcal{N}(0, \mathbf{Q})$. In discrete form one can write

$$\mathbf{x}_{d,k+1} = f(\mathbf{x}_{d,k}) + \mathbf{v}_k \tag{3.5}$$

and one must determine the statistics of $\mathbf{v}_k$. To do so, consider the equations of deck motion for small angular displacements, which can be obtained from Equation 2.10 to Equation 2.21 as

$$\dot{\mathbf{x}}_d = \begin{bmatrix} \mathbf{0}_6 & \mathbf{I}_6 \\ \mathbf{0}_6 & \mathbf{0}_6 \end{bmatrix} \mathbf{x}_d + \begin{bmatrix} \mathbf{0}_6 \\ \mathbf{I}_6 \end{bmatrix} \mathbf{F}_d \tag{3.6}$$

Using a zero-order hold to discretize the equations of motion gives

$$\mathbf{x}_{d,k+1} = \begin{bmatrix} \mathbf{I}_6 & \Delta t \mathbf{I}_6 \\ \mathbf{0}_6 & \mathbf{I}_6 \end{bmatrix} \mathbf{x}_{d,k} + \begin{bmatrix} \frac{\Delta t^2}{2} \mathbf{I}_6 \\ \Delta t \mathbf{I}_6 \end{bmatrix} \mathbf{F}_d \tag{3.7}$$

Thus $\mathbf{v}_k \sim \mathcal{N}(0, \bar{\mathbf{Q}})$ with

$$\bar{\mathbf{Q}} = \begin{bmatrix} \frac{\Delta t^2}{2}\mathbf{I}_6 \\ \Delta t \mathbf{I}_6 \end{bmatrix} \mathbf{Q} \begin{bmatrix} \frac{\Delta t^2}{2}\mathbf{I}_6 & \Delta t \mathbf{I}_6 \end{bmatrix} \tag{3.8}$$

Finally, it is assumed that $\mathbf{Q}$ is diagonal (i.e. the process noise that models wave acceleration is uncorrelated in each of its components), so that

$$\mathbf{Q} = \begin{bmatrix} \sigma_u^2 & 0 & 0 & 0 & 0 & 0 \\ 0 & \sigma_v^2 & 0 & 0 & 0 & 0 \\ 0 & 0 & \sigma_w^2 & 0 & 0 & 0 \\ 0 & 0 & 0 & \sigma_p^2 & 0 & 0 \\ 0 & 0 & 0 & 0 & \sigma_q^2 & 0 \\ 0 & 0 & 0 & 0 & 0 & \sigma_r^2 \end{bmatrix} \tag{3.9}$$

The choice of $\sigma_{(\cdot)}$, expected standard deviation of acceleration for the given component, is important. If it is too small then the modeled deck kinematics will have overly strong confidence in the (incorrect) assumption of constant acceleration. If it is too large the modeled deck kinematics will have such high uncertainty that they will not play a role in deck state estimation. Recall that for sinusoidal deck motion

$$F_{d_{(\cdot)}}(t) = -A_{(\cdot)}\omega_{(\cdot)}^2 \sin\left(\omega_{(\cdot)}t + \varphi_{(\cdot)}\right) \tag{3.10}$$

Thus the peak expected acceleration is $A_{(\cdot)}\omega_{(\cdot)}^2$. Both wave amplitude and frequency depend on sea state, and these are not constant values for any given sea state. Table 2.2 gives expected mean magnitudes and variances for sea states 1, 5, and 7. However, merely choosing the expected wave amplitude and mean wave frequency for a given sea state and computing expected acceleration will result in a conservative prediction of wave excitation. By choosing

$$\sigma_{(\cdot)} = \left(A_{(\cdot)}^{nom} + 3\sigma_A\right)\left(\omega_{(\cdot)}^{nom} + 3\sigma_\omega\right)^2 \tag{3.11}$$

will ensure that a broad range of possible amplitudes and frequencies for a particular sea state are covered.

Combined with the deck kinematics, $\bar{\mathbf{Q}}$ is used in the prediction step of the

UKF algorithm given in Figure 2.7.

3.1.2 Vision Update

Measurements from the camera are used in the measurement update step of the UKF. The modified pinhole projection model of Section 2.2.3 is written compactly as

$$\mathbf{z}_{cam} = g(\mathbf{x}_d, \mathbf{x}_h) + \mathbf{n}_c \tag{3.12}$$

It is assumed that measurement noise $\mathbf{n}_c$ is zero-mean Gaussian and that noise is uncorrelated across bearings, so that

$$\mathbf{n}_c \sim \mathcal{N}(0, \mathbf{R}) \tag{3.13}$$

with

$$\mathbf{R} = \sigma_{cam}^2 \mathbf{I} \tag{3.14}$$

3.1.3 Choice of Deck States

When simulating a system, it is important to choose the best set of states in order to fully describe the motion. One wants just enough states to fulfill the EOMs, but not too many states that computations become too intensive such that real-time applications become impossible. The only set of chosen states are the deck states needed for state estimation and prediction since UAV states are given by a GPS/INS. Recall the pertinent states needed from Table 2.1. These states have been determined to be the minimum spanning set to accomplish all the tasks laid out in this thesis. If the mission goals or problem statement were to be altered then the deck states may be altered as well. However the UKF algorithm is indifferent to the set of states being estimated, so long as the process model and kinematics from Chapter 2 are updated accordingly. It is also important to note that with the current set of states, the system is able to run faster than real time.

3.2 Data Association

Data association is a critical component of the deck state estimator. Failure to correctly associate measured bearings with the corresponding marker will almost certainly lead to divergence of the deck state estimator.

Data association is an example of an assignment problem. This class of problems has been extensively studied in the computer science literature and in robotics applications (especially problems related to simultaneous localization and mapping, or SLAM) [19, 20, 4].

In this research, data association is computed by comparing the pixel location of a marker in the current image frame with pixel locations of markers in the previous frame. Close matches are assumed to come from the same marker. In this case "close" is computed as the Mahalonobis Distance:

$$d_{nm} = (\mathbf{z}_n - \mathbf{z}_m)^T \mathbf{P}_{mm}^{-1} (\mathbf{z}_n - \mathbf{z}_m) \tag{3.15}$$

Here $\mathbf{z}_m$ is the expected pixel location of a marker from the previous frame in the current frame and $\mathbf{z}_n$ is the measured pixel location of a marker in the current frame. The matrix $\mathbf{P}_{mm}$ represents the uncertainty of the expected marker position. The quantity d_{nm} thus represents the distance (scaled by uncertainty) between a measured marker location and the expected marker location.

This distance is computed for all possible combinations, leading to an $n \times m$ distance matrix:

$$\mathbf{D} = \begin{bmatrix} d_{11} & d_{12} & \cdots & d_{1m} \\ d_{21} & d_{22} & \cdots & d_{2m} \\ \vdots & & & \vdots \\ d_{n1} & \cdots & \cdots & d_{nm} \end{bmatrix} \tag{3.16}$$

The problem now is to compute the assignments that minimize the overall cost. One approach is to begin with the top row and assign the markers in turn based on minimum distance. This "greedy" approach is brittle, however, and may lead to incorrect assignment in cases of ambiguity (i.e. similar distances for several possible assignments).

A better approach is to minimize the total cost. In large assignment problems (with tens or hundreds of markers) it can quickly become computationally pro-

hibitive to brute force this problem (i.e. compute cost of all possible assignments, choose the lowest net cost).

However, the Munkres method [14] can be used to quickly find the optimal data association based on the Mahalonobis distances. The Munkres algorithm is traditionally used to determine a best job-agent placement, but with some minor alterations, the algorithm works equally well correlating lights from frame to frame. The Munkres method was published by mathematician Harold Kuhn, but based on the works of earlier mathematicians Dénes Kőnig, Jenő Egerváry, and finally James Munkres [14].

The positives of this method is that it is robust, magnitude indifferent, and works when a light may enter or leave the field of view. This is a big positive, since the data association can continue uninhibited when the number of markers in view changes. However, deck state estimation requires a minimum of three markers in view, but to improve performance and observability four markers were used in this thesis.

3.3 Deck Estimate Initialization

In Chapter 2 the kinematics of deck motion were described in depth. The UKF uses the previous estimate and incoming measurements to provide a best estimate and associated covariance. An important aspect of this process that hasn't been detailed is how the estimated states are initially computed.

It is assumed that the only a priori information of deck state or outside conditions comes from a single message sent from the ship: providing the UAV with a nominal ship speed, heading, and sea state. Without any other information about deck position or orientation the rest of the states are initialized to zero. Therefore, the initial estimated deck state is defined as,

$$\hat{\mathbf{x}}_{\mathbf{d,0}} = [0\ 0\ 0\ 0\ 0\ \psi_0\ u_0\ v_0\ 0\ 0\ 0\ 0\ 0]^T$$

Along with the initial deck estimate, an initial deck covariance is computed. This is assumed to be diagonal (uncorrelated), with the magnitude of each component dependent on sea state. For each component of the deck state, the standard

deviation is set to equal the root mean square value of the expected amplitude due to wave motion. For position and orientation states

$$\mathbf{P}_{0_{(\cdot)}} = \frac{A^2_{nom,(\cdot)}}{2} \tag{3.17}$$

and for velocity and angular rate states

$$\mathbf{P}_{0_{(\cdot)}} = \frac{A^2_{nom,(\cdot)}\omega^2_{nom,(\cdot)}}{2} \tag{3.18}$$

Expected amplitudes and frequencies for all sea states simulated in this thesis will be defined in Section 4.2.1, which describes simulation conditions.

Chapter 4

Estimator Simulation Results

This chapter details the results of simulations of six degree of freedom deck state estimation. These simulations provide the opportunity to prove that the estimator and data association techniques are both accurate as well as robust enough to be used across a range of sea conditions and external environments.

Simulation results are utilized to show that the estimator is capable of deck state estimation in terms of accuracy, precision, and consistency. Results for a representative run with a standard sea state show that the system is accurate. Presenting representative run results for a variety of wave motion models shows that the system is precise. Finally, using Monte Carlo simulations can show the consistency of the system working in various sea states or wave conditions. In addition, showing these results for all three wave motion models proves the that the estimator need not rely on a specific wave motion model in order to estimate deck states.

4.1 Helicopter Kinematics

Since the focus here is on estimation (and not flight control or path planning) a kinematic model is used for the helicopter. Recall from Chapter 2 the vehicle state vector:

$$\mathbf{x}_h = [x_h \; y_h \; z_h \; \phi_h \; \theta_h \; \psi_h \; u_h \; v_h \; w_h]^T$$

The vehicle also has control vector:

$$\mathbf{u}_h = [p_h \; q_h \; r_h \; T_x \; T_y \; T_z]^T$$

Where $\mathbf{u}_h$ represents the vehicle control vector. $[T_x \; T_y \; T_z]$ represents the thrust vector components in the x, y, and z directions. Thus it is implicitly assumed that an on-board controller could follow angular rate commands and could compute a desired magnitude and direction of the net thrust vector (within constraints). EOMs using small angle approximations found to be:

$$\begin{aligned}
\dot{x}_h &= u(\cos\psi_h) - v_h(\sin\psi_h) + w_h(\theta_h\cos\psi_h + \phi_h\sin\psi_h) && (4.1)\\
\dot{y}_h &= u_h(\sin\psi_h) - v_h(\cos\psi_h) + w_h(\theta_h\sin\psi_h - \phi_h\cos\psi_h) && (4.2)\\
\dot{z}_h &= (-\theta_h)u_h + (\phi_h)v_h + w_h && (4.3)\\
\dot{\phi}_h &= p_h - (\theta_h)r_h && (4.4)\\
\dot{\theta}_h &= q_h - (\phi_h)r_h && (4.5)\\
\dot{\psi}_h &= (\phi_h)q_h - r_h && (4.6)\\
\dot{u}_h &= -(w_h q_h - v_h r_h) + T_x/m - g\theta_h && (4.7)\\
\dot{v}_h &= -(u_h r_h - w_h p_h) + T_y/m + g\phi_h && (4.8)\\
\dot{w}_h &= -(v_h p_h - u_h q_h) + T_z/m + g && (4.9)
\end{aligned}$$

In the vehicle acceleration equations, g represents gravitational acceleration at the Earth's surface. $[T_x \; T_y \; T_z]$ represent components of the aerodynamic forces and thrust vector.

Now the vehicle kinematic design is fully outlined, simulation conditions can be shown.

4.2 Simulation Conditions

The ship is traveling at a nominal speed of 3 m/s (5.8 kts). The helicopter begins from a point 250 meters behind and 100 meters above the ship, and it travels at a constant speed of 14.5 m/s (28 kts) in a straight line towards the ship deck. The simulation starts at time zero and ends at t = 20 seconds, when the helicopter is

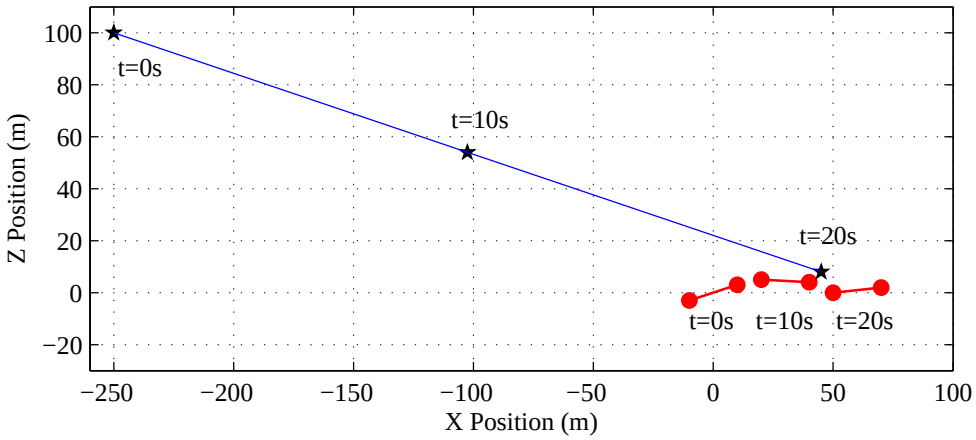

Figure 4.1. A two dimensional schematic of vehicle approach and deck position change vs. time

UAV *positions are denoted by star, deck marker positions are denoted by circles. Labels correspond to time since start of the simulation. Deck motion due to waves is exaggerated for this schematic.*

approximately 15 meters behind and 8 meters above the ship deck.

The four deck markers were arranged in a square pattern on the deck surface around the origin of the deck body frame. This square had a baseline of 20 meters, and one marker was located in each of the corners.

A schematic of the specific simulation conditions is shown in Figure 4.1

4.2.1 Sea State Conditions

The simulation used a given sea state to generate sea conditions for the deck to be subject to. For each run a new random sea condition was generated using the statistics in Table 4.1. For each of the six degrees of freedom undergoing wave forces, a mean wave amplitude and frequency are given as well as associated covariances. This covariance information is used to randomize the wave properties for each degree of freedom for each run. For the sinusoidal model these are the properties used to determine and randomize wave motion.

For the stochastic model the mean wave amplitude generated was used as the peak wave height ($h_{1/3}$). From this a power spectrum could be generated, a peak frequency could be found, and then the proper set of bandwidth frequencies could

then be computed.

Table 4.1. Wave State Simulation Information for Sea states 1, 5, 7

Component	Mean Amp.	Amp. Variance	Mean Period	Period Variance
		Sea state 1		
x	0.2 m	0.1 m^2	5 sec	1 sec^2
y	0.2 m	0.1 m^2	5 sec	1 sec^2
z	0.5 m	0.2 m^2	5 sec	1 sec^2
ϕ	4°	2°^2}	5 sec	1 sec^2
θ	1°	1°^2}	5 sec	1 sec^2
ψ	1°	1°^2}	5 sec	1 sec^2
		Sea state 5		
x	1 m	0.5 m^2	12 sec	3 sec^2
y	1 m	0.5 m^2	12 sec	3 sec^2
z	2.5 m	1 m^2	12 sec	3 sec^2
ϕ	12°	3°^2}	12 sec	3 sec^2
θ	5°	2°^2}	12 sec	3 sec^2
ψ	3°	1°^2}	12 sec	3 sec^2
		Sea state 7		
x	2.6 m	1.3 m^2	17 sec	4 sec^2
y	2.6 m	1.3 m^2	17 sec	4 sec^2
z	6.5 m	2.5 m^2	17 sec	4 sec^2
ϕ	35°	9°^2}	17 sec	4 sec^2
θ	12°	3°^2}	17 sec	4 sec^2
ψ	4°	3°^2}	17 sec	4 sec^2

4.2.2 UKF Parameters

With the given sea state and wave properties for a particular run, filter process noise magnitude was computed using Equation 3.11. From Equation 3.14, camera noise covariance (σ^2_{cam}), was chosen to equal ($\frac{\pi}{180}$ radians)^2.

It is important to reiterate that vehicle states are assumed to be known with a high level of precision. In reality, accuracy in the determination of helicopter orientation will be limited to a standard deviation of approximately 1° to 2°. However, this uncertainty can be included in the camera bearing measurement uncertainty. Noise in the UAV position estimate will have a much smaller impact on performance than attitude uncertainty.

Performances for both the representative run at sea state 5, and various Monte Carlo simulations will be presented for the sinusoidal wave model and stochastic wave model. For each of these models representative run analysis will be done first (Section 4.3.1, Section 4.4.1), followed by Monte Carlo result analysis (Section 4.3.2 ,Section 4.4.2). While representative run analysis is only performed for sea state 5, Monte Carlo analysis was performed for sea states 1, 5, and 7.

The fast ferry ship model is only valid for moderate wave motion, equivalent to sea state 4. Representative run analysis (Section 4.5.1) and Monte Carlo analysis (Section 4.5.2) for this model was done for that sea state only.

4.3 Sinusoidal Wave Motion Model

4.3.1 Representative Run Analysis (Sinusoidal Wave Model)

Figure 4.2 and Figure 4.3 shows all true deck states versus the estimated deck states for a representative run at sea state 5. Included in these plots are the $\pm 2\sigma$ boundaries on the estimate.

Figure 4.2(a) shows deck positions are estimated and tracked closely. By the end of the simulation (20 seconds), the estimate and truth are nearly identical; with only a 0.369 meter error at the end of this run. Also the estimator has a high confidence in the knowledge of these states, since the covariance continually converges during the simulation. Attitude estimation in (Figure 4.2(b)) shows similar behavior, with an error of only 0.571°. The estimator is able to closely follow the sinusoidal model, and keep the estimate close to truth.

Analysis of deck velocity and rotation rate estimation, Figure 4.3(a) and Figure 4.3(b) does show adequate estimation. While these estimates are not as accurate as the positions and orientations, they are still well within the covariance bounds. The velocity error has magnitude 0.126 meters per second and there is an angular rate error of 0.93° per second. While the estimator doesn't track these states as precisely, it is clear that the general behavior of these states is captured. Also it is evident that the estimator is aware that the knowledge of these states is not perfect, which is shown by the covariance bounds hardly converging with the

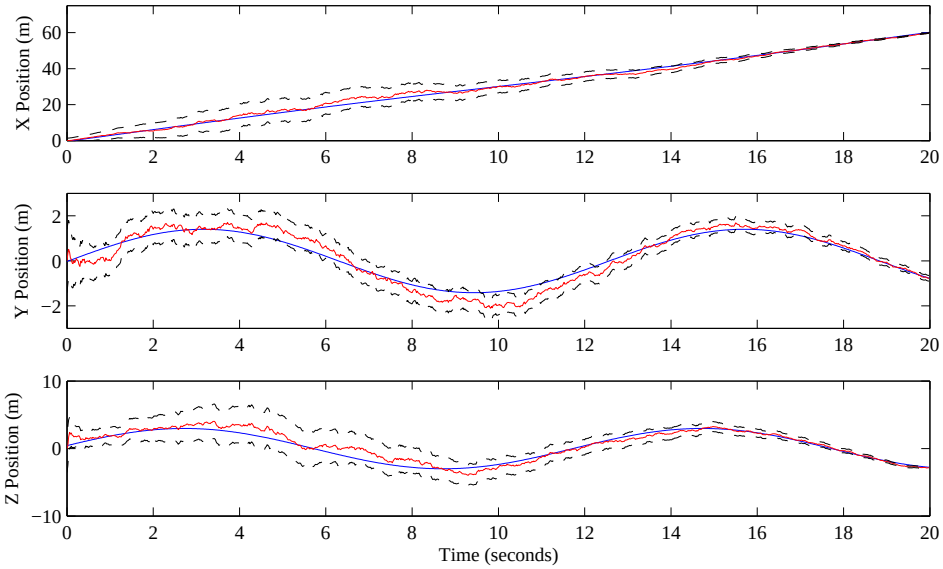

(a)

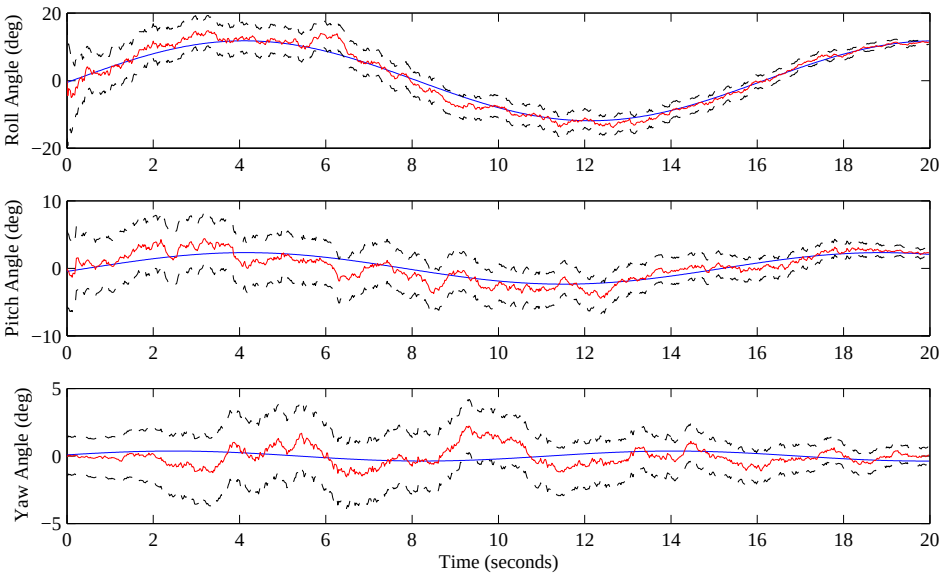

(b)

Figure 4.2. Representative Run Position and Orientation Estimation (Sinusoidal Wave Model)

Representative run position and orientation estimation using the sinusoidal wave model. True state shown in blue, estimated state is shown in red, $\pm 2\sigma$ bounds are shown as dashed lines.

length of observation.

With the estimator shown to estimate deck states to an acceptable accuracy, and also have good knowledge of the uncertainty in the estimates, attention can be turned to a visual representation of how the estimator is performing with time.

Using the known estimated deck state $\hat{\mathbf{x}}_d$ and deck state covariance $\mathbf{P}_d$, spatial covariance of marker positions can be computed. This marker covariance is not used for any further computation, but does provide a strong visual depiction of estimator behavior by showing the uncertainty of determined marker positions.

Figure 4.4 displays how the three standard deviation error ellipsoids for each of the four markers evolves over time. Also included in each plot is the true deck outline (in blue) and estimated deck outline (in red). This figure shows the error ellipsoids, deck state, and deck estimate at times of 0, 4, 8, 12, 16, and 20 seconds.

This figure shows some how the system expects errors in the spatial estimation of marker position initialize and evolve with time. Initially it is evident that the estimator believes there is more error in the z direction than the other two position states. This is expected, since z wave magnitude is the largest, and thus the covariance on z position is the largest of the position states. By 4 seconds in the estimator appears to have better knowledge of z position, and x position appears to be the dominant error. One can observe the ellipsoids elongating along the x axis.

This covariance growth is caused by the vision measurement noise model used. Since constant Gaussian noise was used on all bearing measurements, the noise has a larger effect on position estimation at further distances than when the UAV is closer to the deck. This is evidenced by the fact that as the vehicle continues to approach, the error ellipsoids consistently shrink in all directions. By the end of the simulation, the estimate and truth are hard to distinguish from one another, and the error ellipsoids just barely envelope the dots representing the markers.

This concludes the representative run analysis for the sinusoidal model.

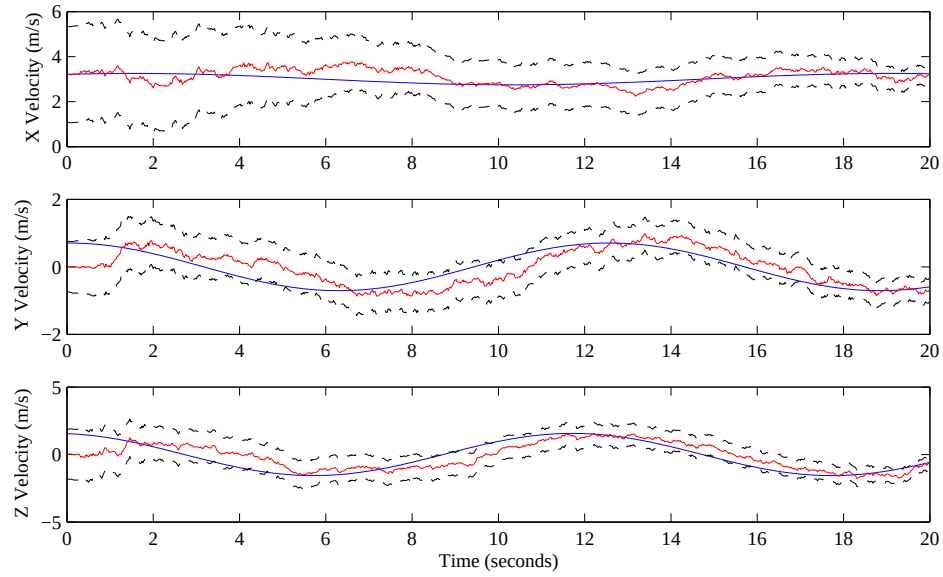

(a)

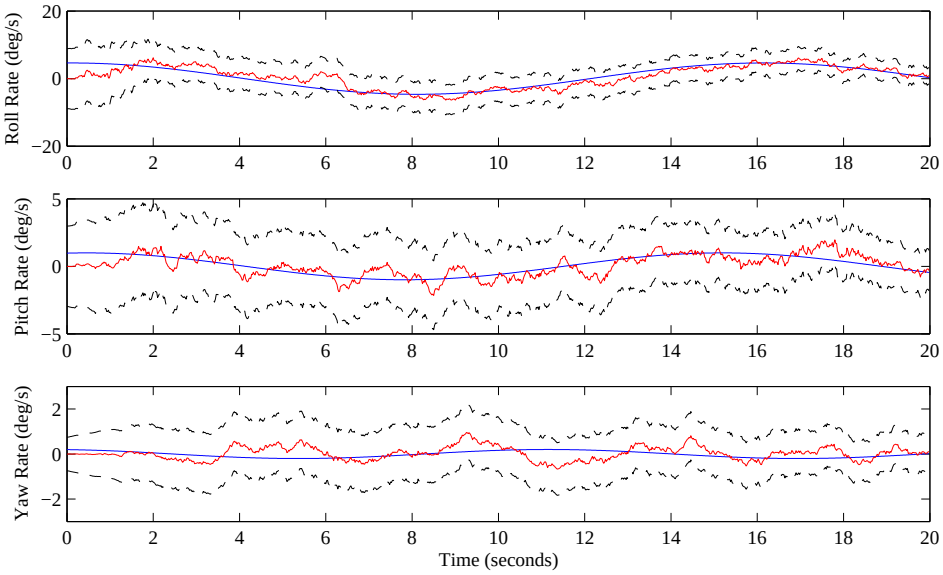

(b)

Figure 4.3. Representative Run Velocity and Angular Rate Estimation (Sinusoidal Wave Model)

Representative run position and orientation estimation using the sinusoidal wave model. True state shown in blue, estimated state is shown in red, $\pm 2\sigma$ bounds are shown as dashed lines.

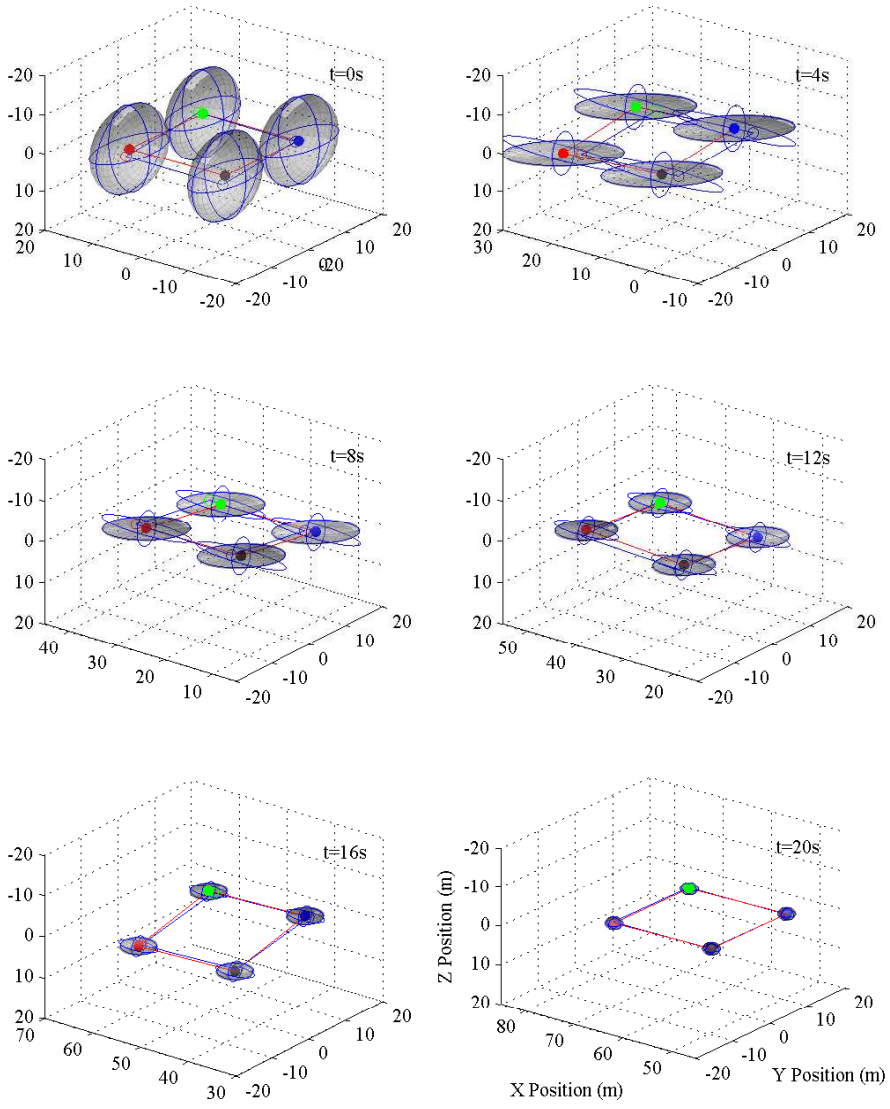

Figure 4.4. Analysis of Deck Marker Error Ellipsoids (Sinusoidal Wave Model)
This plot shows the 3σ error ellipsoids for each individual deck marker. Plots are shown for 6 times within the simulation (t=0, 4, 8, 12, 16, 20 seconds). The red box corresponds to estimated deck position, and the blue box is the true deck position. Open dots represent the estimated marker positons, while filled dots represent true marker positions. Each marker is colored seperately in order to more easily identify them individually between plot.

4.3.2 Monte Carlo Simulation Results (Sinusoidal Wave Model)

When analyzing Monte Carlo results, the idea is not to analyze data on a run by run basis, but to look at the overarching characteristic behaviors of the system. It is possible to characterize the basic properties of the system by looking at the average result from many runs. By looking at data across many simulations wave randomization and noise become less prominent in the results. One can also show the maximum and minimum outliers for that set of runs. For Monte Carlo simulations, overall error characteristics will be examined, as well as error characteristics for all the state groups (position, orientation, velocity, angular rates).

The way to read all the plots pertaining to Monte Carlo results are as a time history of true mean error (blue), bounded by the maximum and minimum error (gray area). This is compared against the mean estimated error (red).

Figure 4.5 shows how the true and estimated error of the total deck state evolves with time, for various sea states. There is a definite correlation in performance to sea state. The estimator initially is cautious about the estimate when far away, but as the approach continues the true error becomes comparable to the estimated error. This is because at larger distances measurement noise has a larger effect on the deck estimate, so it takes some time until the UAV gets close enough to the deck for the estimator to overcome the noise. It is important to note that as sea state increases, the estimator does show a trend in becoming slightly overconfident in the overall error estimation. This is to be expected: as sea state increases so does the magnitude of the disturbances acting upon the deck, and thus the unmodeled dynamics have a larger effect on estimation accuracy.

The same analysis performed for overall deck state error behavior can now be extended to each group of states. With this analysis estimator behavior with respect to given state group can be inspected, and the errors involved will have real physical meanings.

Figure 4.6 shows position error behavior versus sea state. These plots look very similar to the total error plots, and indeed the position states are the largest magnitude set of states, and thus tend to drive behavior of the estimator. With each sea state the estimator is able to overcome the initial large error from mea-

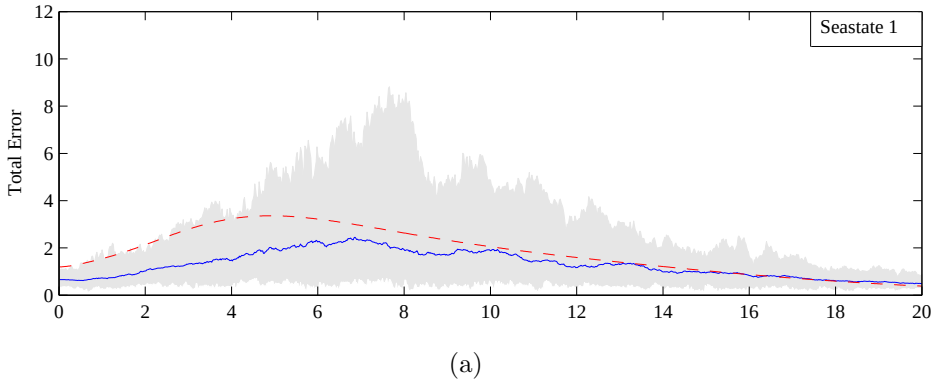

(a)

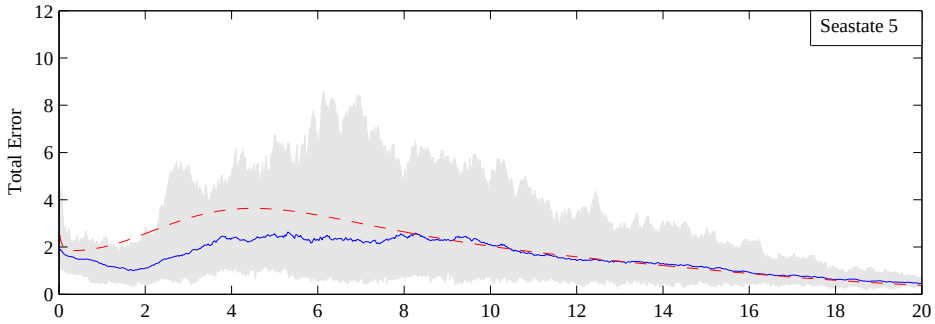

(b)

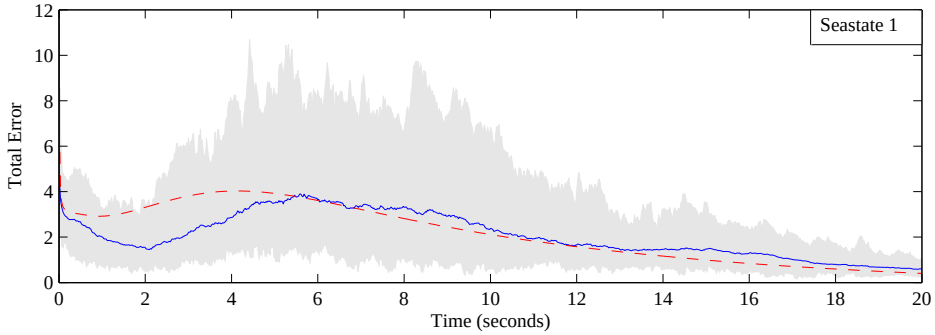

(c)

Figure 4.5. Total Deck State Estimation Error vs. Sea state (Sinusoidal Wave Model) *Estimator total error for sea states 1, 5, 7. The grey region shows maximum and minimum bounds of true error. The blue line shows mean true error, and the red dashed line shows estimated total variance (i.e.* $\sqrt{\mathrm{Tr}\mathbf{P}}$*).*

surement noise, and accurately estimate error by approximately halfway through the simulation. Similarly to the total error plot, the estimator does show some overconfidence in the position estimation for all sea states. However, these errors are small.

Attitude estimation was shown to be very strong in the representative run, and Figure 4.7 shows that error estimation for these states is accurate as well. For sea states 1 and 5 the estimated error quickly closes in on truth, and remains on top of it through the end of the simulation. There is almost no overconfidence in the attitude estimation for sea states up to 5. Sea state 7 does not fare quite as well; consistently the estimator is overconfident of the accuracy of the estimation. While this error is small, approximately 2° in magnitude, it is persistent for a majority of the simulation.

Velocity estimations, from Figure 4.8, show very strong knowledge in the velocity error at lower sea states. Both sea states 1 and 5 start with a significant difference betweent the true and estimated error. However, the estimator overcomes this difference and both sea states have well known velocity errors by the end of simulation. At higher sea states, like the attitude estimation, the estimator overconfidently estimated deck velocity.

Rotation rate estimation (Figure 4.9) appears to be the most difficult set of states for the estimator to get a grasp of uncertainty in. While the estimator does succeed at sea state 1, sea states 5 and 7 again exhibit overconfidence in the estimate. Again though these errors are small, with the estimator only overconfident by 3° per second.

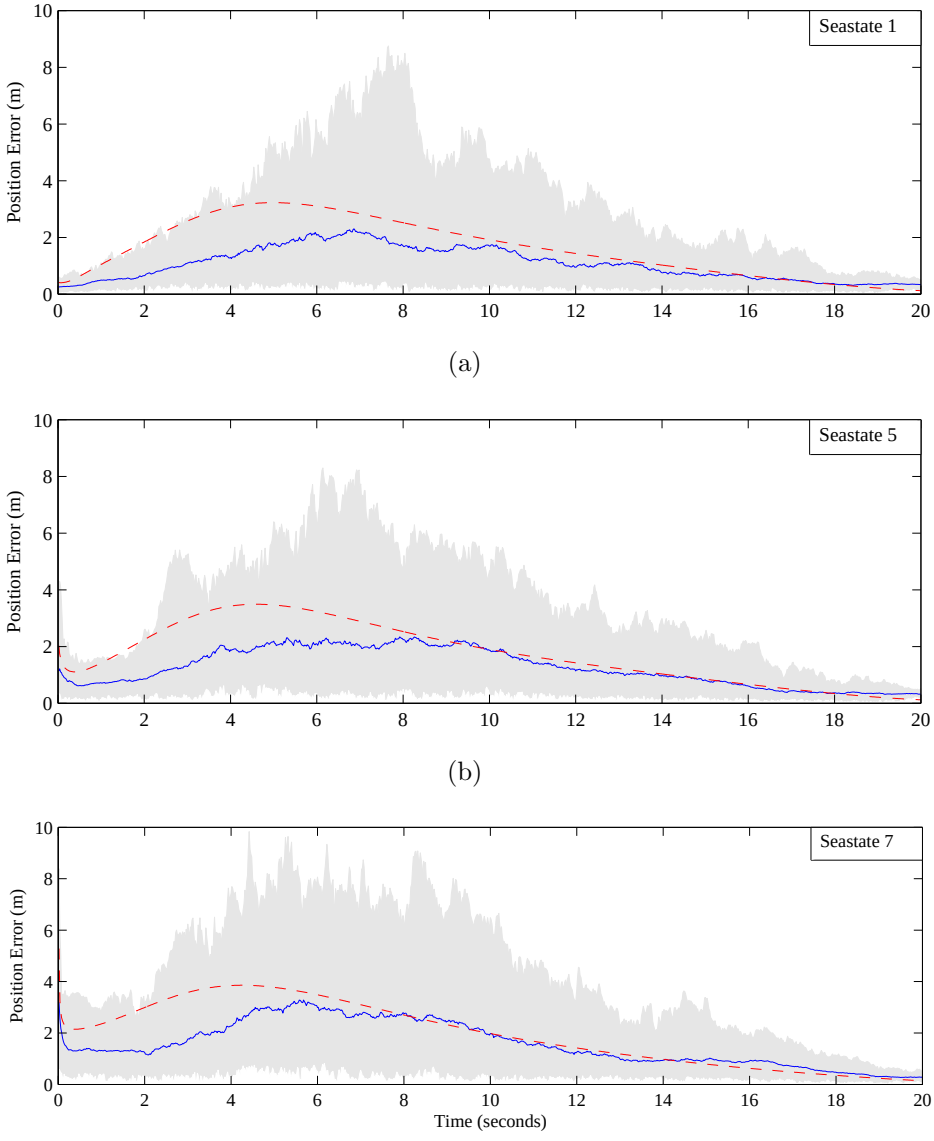

Figure 4.6. Position State Estimation Error vs. Sea state (Sinusoidal Wave Model) *Estimator position error for sea states 1, 5, 7. The grey region shows maximum and minimum bounds of true error. The blue line shows mean true error, and the red dashed line shows estimated total variance (i.e.* $\sqrt{\mathrm{Tr}\mathbf{P}}$*).*

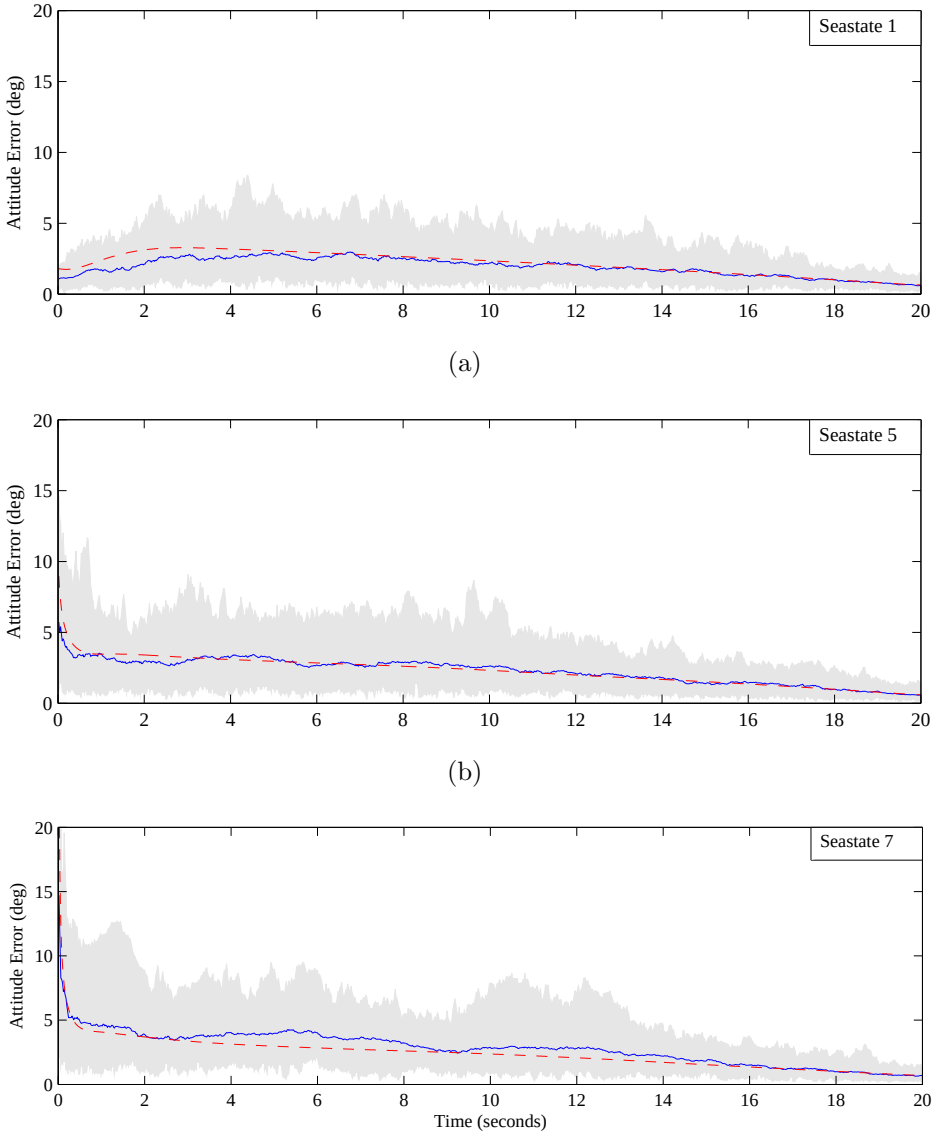

Figure 4.7. Orientation State Estimation Error vs. Sea state (Sinusoidal Wave Model) *Estimator attitude error for sea states 1, 5, 7. The grey region shows maximum and minimum bounds of true error. The blue line shows mean true error, and the red dashed line shows estimated total variance (i.e.* $\sqrt{\mathrm{Tr}\mathbf{P}}$*).*

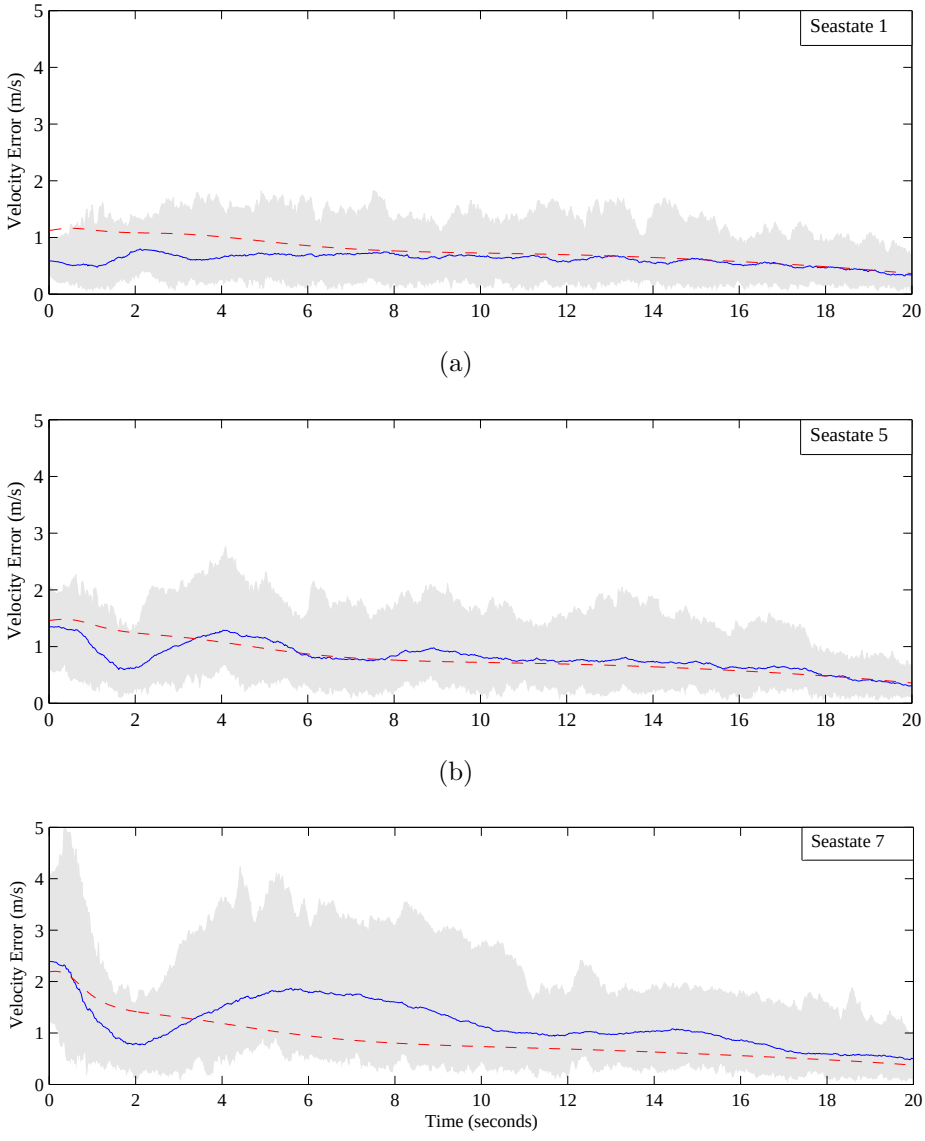

Figure 4.8. Velocity State Estimation Error vs. Sea state (Sinusoidal Wave Model) *Estimator velocity error for sea states 1, 5, 7. The grey region shows maximum and minimum bounds of true error. The blue line shows mean true error, and the red dashed line shows estimated total variance (i.e.* $\sqrt{\mathrm{Tr}\mathbf{P}}$*).*

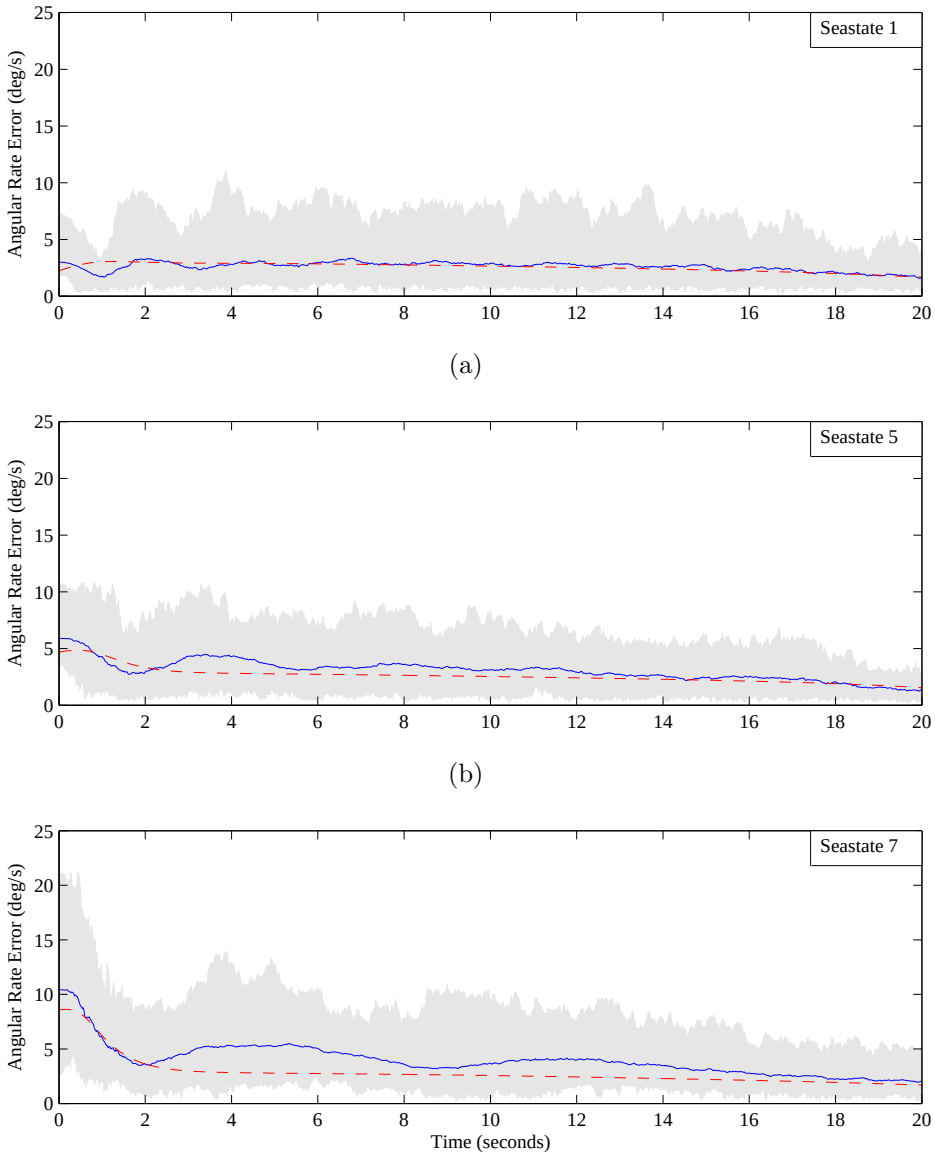

Figure 4.9. Angular Rate State Estimation Error vs. Sea state (Sinusoidal Wave Model)

Estimator angular rate error for sea states 1, 5, 7. The grey region shows maximum and minimum bounds of true error. The blue line shows mean true error, and the red dashed line shows estimated total variance (i.e. $\sqrt{\mathrm{Tr}\mathbf{P}}$*).*

4.4 Stochastic Wave Motion Model

4.4.1 Representative Run Analysis (Stochastic Wave Model)

With analysis of estimator behaviors for the sinusoidal model complete, the results of the estimator performance with respect to the more complex stochastic wave motion model can be shown. The same plots for the sinusoidal model will be shown here for the stochastic results.

Figure 4.10 shows the results of position and orientation estimation for the deck undergoing stochastic wave motion. While the motion in both sets of states is certainly more random, the estimator is able to handle this type of wave motion. All positions are accurately tracked, and attitudes estimates nearly lie on the truth. The position is known to within 0.425 meters of accuracy. It is evident that the estimator has strong knowledge of the attitude estimates as well. By the end of the simulation the error on these states is just 0.518°. As previously seen in the sinusoidal representative run results the covariance bounds on all six of these states continuously shrink as the observation time increases.

Figure 4.11 shows that the stochastic model simulation results exhibit a similar loss of accuracy in velocity and angular rate estimation when compared to positions or attitudes. It appears the more random wave motion of the stochastic model proves more challenging for the estimator to track. Velocities are estimated adequately (0.403 meters per second error), and a majority of the motion is captured within the standard deviation boundaries. Attitude rate estimation appears to be the toughest state to track. While the estimator does seem to get a mean value for each rotation rate, it is not able to track the high frequency motion that defines these states. The final error on attitude rates is 5.98° per second. However, even with the overall error the estimator does appear to keep large enough uncertainty boundaries on these states, and a majority of the error is captured within them.

Keeping consistent with the sinusoidal model, an analysis of Figure 4.12 shows how the estimate of ellipsoid positions changes over the length of the simulation. The estimator again initializes with a large estimate in the z direction. All four

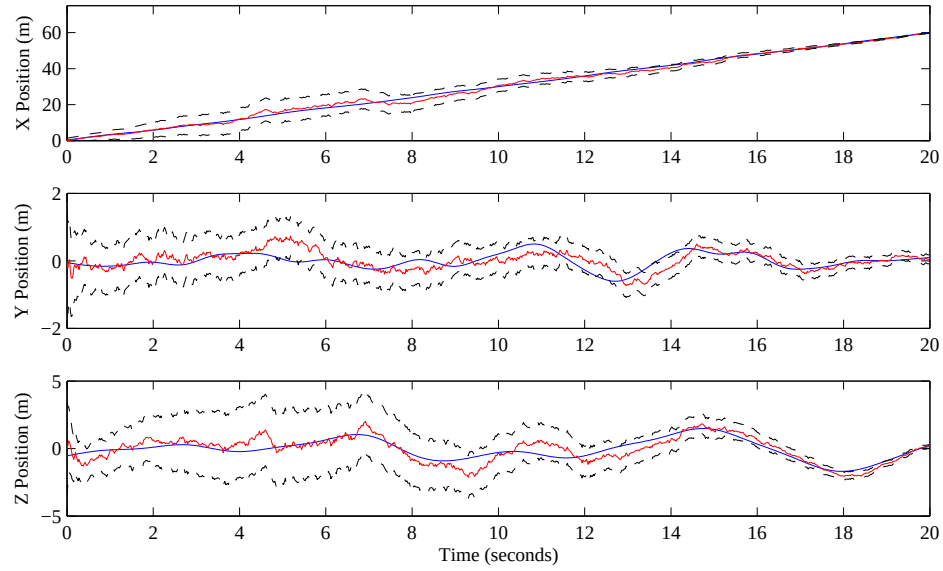

(a)

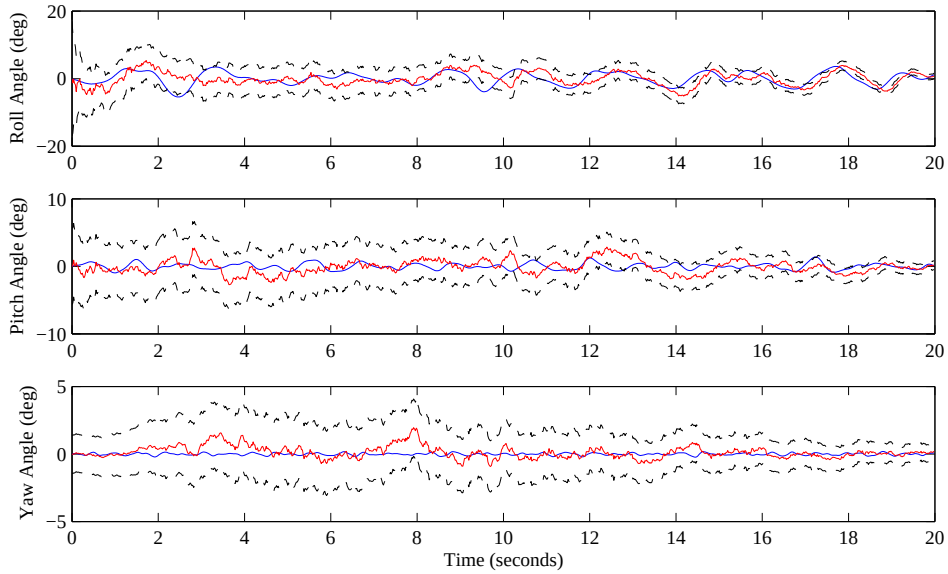

(b)

Figure 4.10. Representative Run Position and Orientation Estimation (Stochastic Wave Model)

Representative run position and orientation estimation using the stochastic wave model. True state shown in blue, estimated state is shown in red, $\pm 2\sigma$ bounds are shown as dashed lines.

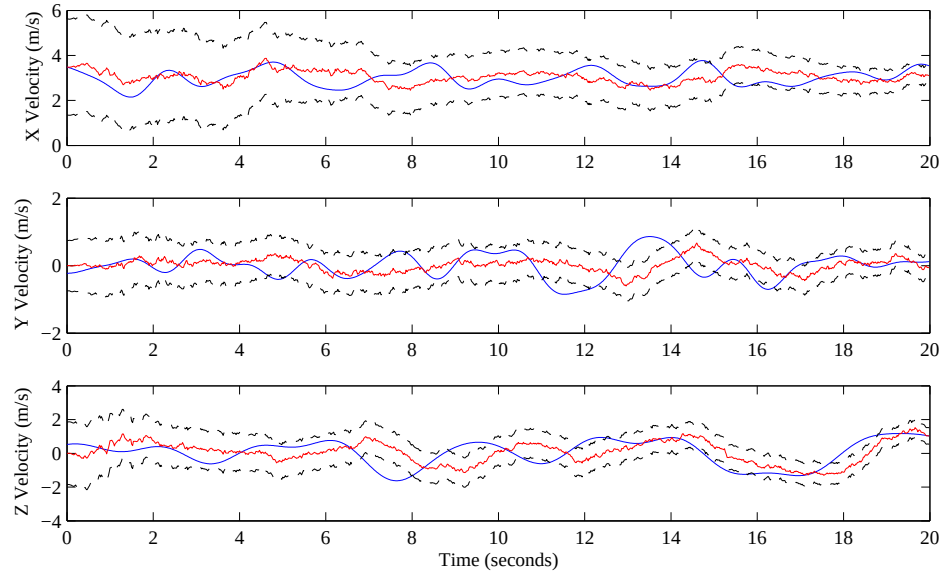

(a)

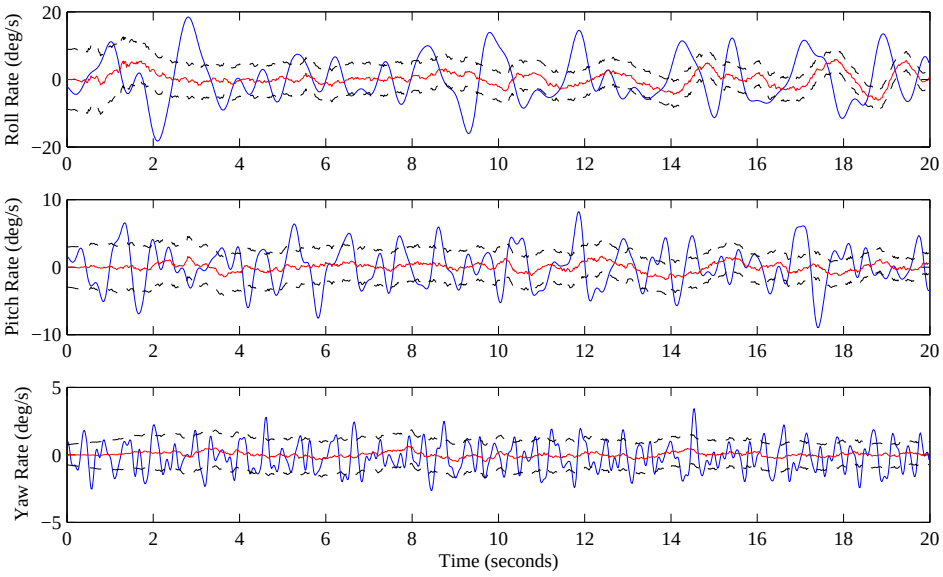

(b)

Figure 4.11. Representative Run Velocity and Angular Rate Estimation (Stochastic Wave Model)

Representative run position and orientation estimation using the stochastic wave model. True state shown in blue, estimated state is shown in red, $\pm 2\sigma$ bounds are shown as dashed lines.

markers have identical error ellipsoids since they are all equidistant from the deck centroid, and no measurements have yet been taken.

Once again the ellipsoids elongate in the x direction while shrinking in the y and z directions. By 12 seconds the deck has a strong confidence in the spatial estimates, and by the end of the simulation, the estimate and truth are nearly identical.

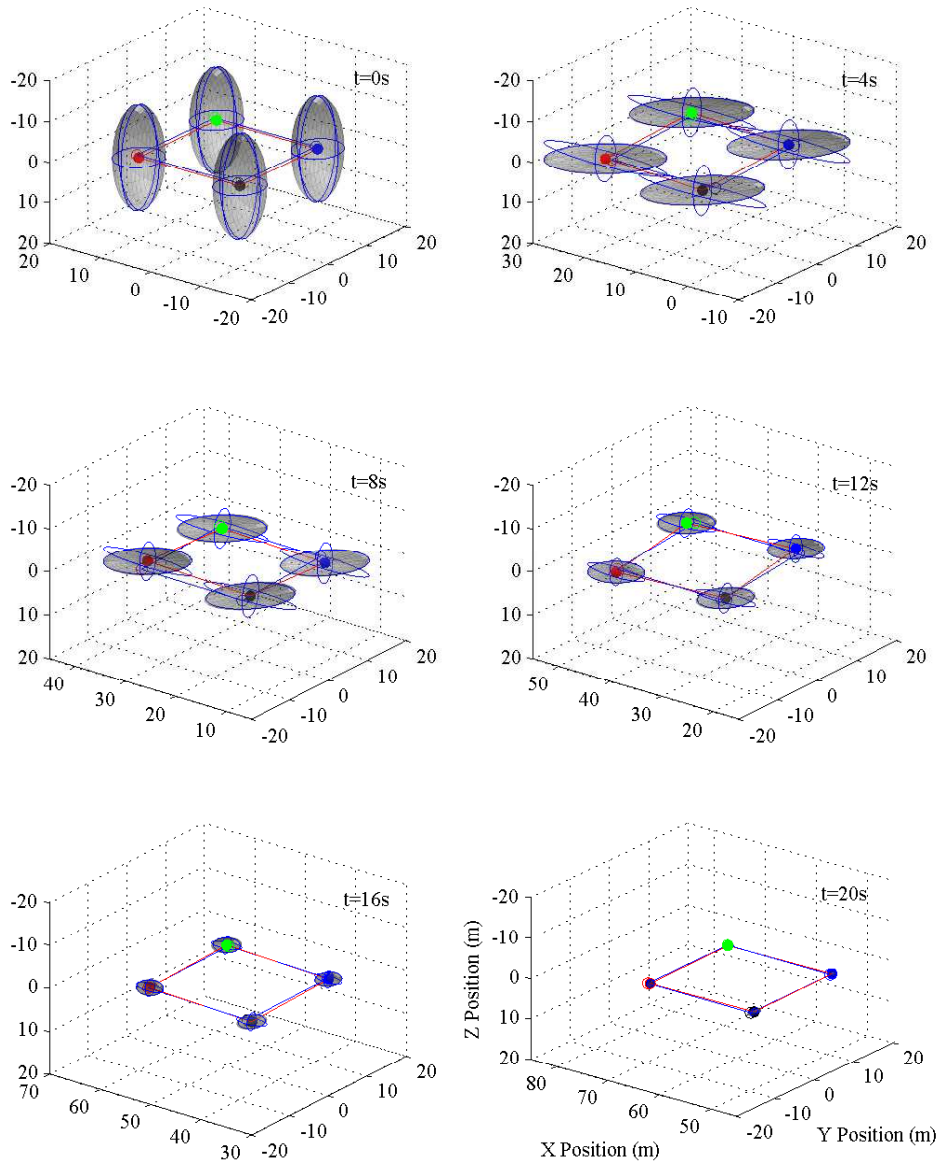

(a)

Figure 4.12. Analysis of Deck Marker Error Ellipsoids (Stochastic Wave Model) *This plot shows the 3σ error ellipsoids for each individual deck marker. Plots are shown for 6 times within the simulation (t=0, 4, 8, 12, 16, 20 seconds). The red box corresponds to estimated deck position, and the blue box is the true deck position. Open dots represent the estimated marker positons, while filled dots represent true marker positions. Each marker is colored seperately in order to more easily identify them individually between plot.*

4.4.2 Monte Carlo Simulation Results (Stochastic Wave Model)

Results of total state error tracking for the stochastic wave model show similar behavior to the sinusoidal model. Figure 4.13 depicts that as the wave disturbance magnitude grows, the estimator becomes overconfident in the estimate; letting the estimated error magnitude fall below the true error magnitude.

Examination of components of the total error can illuminate how confident the estimator is in the measurement of each set of states. Figure 4.14 through Figure 4.17 depict the error characteristics of each subgroup of deck states. Positions again are shown to be the driving states of the system, appearing very similar to total error characteristics. Both position and attitude estimation appear to show slight overconfidence tendencies as sea state increases. However, performance in error estimation of these states is nearly indistinguishable from the sinusoidal model.

Velocity error estimation shows more significant accuracy degradation versus sea state than what was seen from the sinusoidal model. While sea state 1 error is still accounted for properly, sea state 5 and 7 show visible overconfidence in the deck velocity measurements. Angular rate estimation also behaved similar to velocity: with increasing sea state leading to increasing overconfidence.

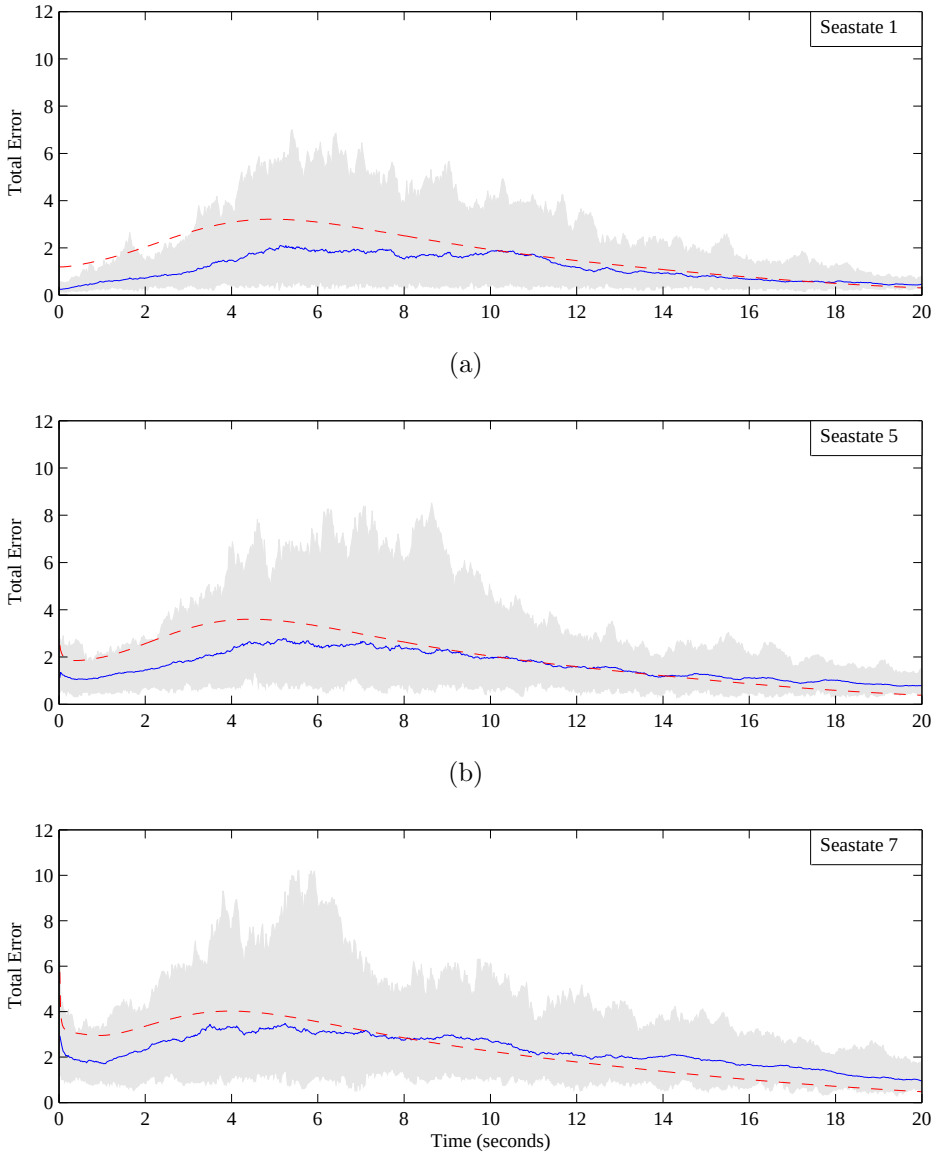

Figure 4.13. Total Deck State Estimation Error vs. Sea state (Stochastic Wave Model) *Estimator total error for sea states 1, 5, 7. The grey region shows maximum and minimum bounds of true error. The blue line shows mean true error, and the red dashed line shows estimated total variance (i.e.* $\sqrt{\mathrm{Tr}\mathbf{P}}$*).*

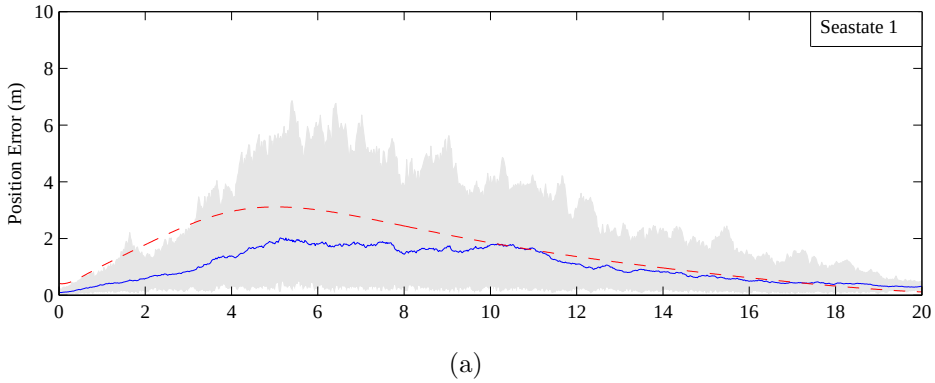

(a)

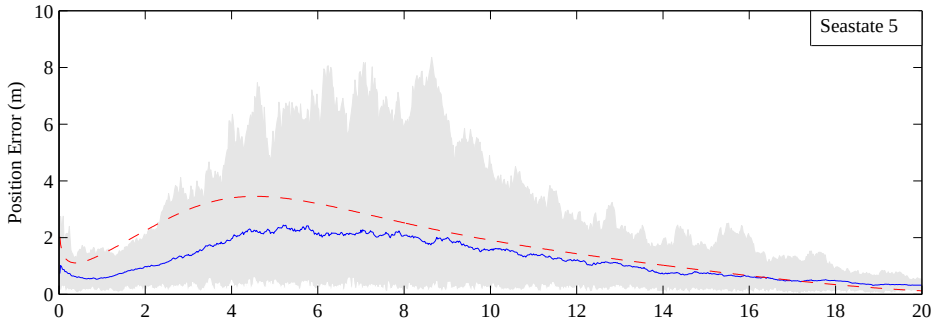

(b)

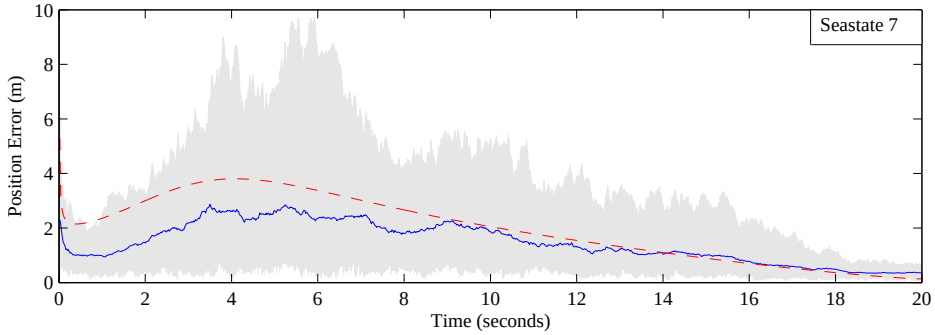

(c)

Figure 4.14. Position State Estimation Error vs. Sea state (Stochastic Wave Model) *Estimator position error for sea states 1, 5, 7. The grey region shows maximum and minimum bounds of true error. The blue line shows mean true error, and the red dashed line shows estimated total variance (i.e.* $\sqrt{\mathrm{Tr}\mathbf{P}}$*).*

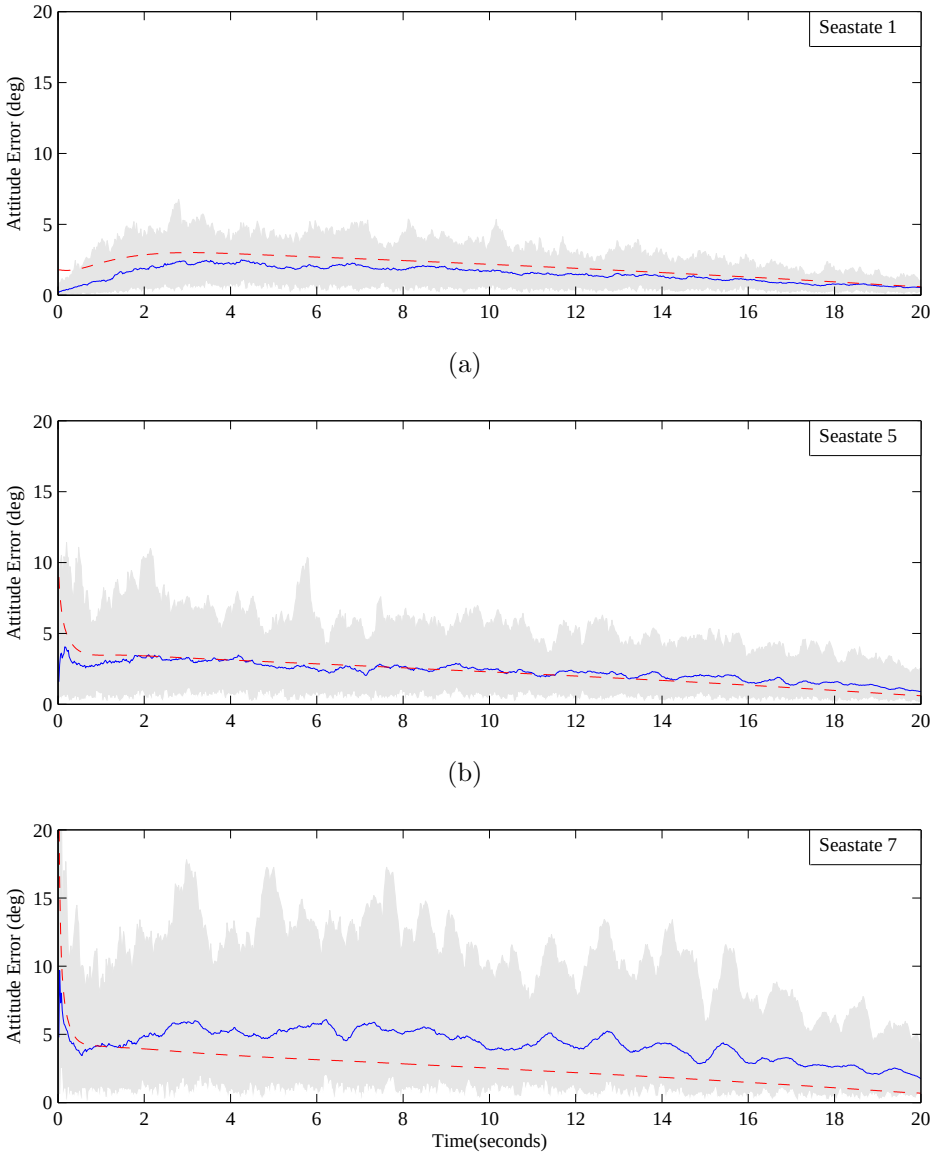

Figure 4.15. Orientation State Estimation Error vs. Sea state (Stochastic Wave Model) *Estimator attitude error for sea states 1, 5, 7. The grey region shows maximum and minimum bounds of true error. The blue line shows mean true error, and the red dashed line shows estimated total variance (i.e.* $\sqrt{\mathrm{Tr}\mathbf{P}}$*).*

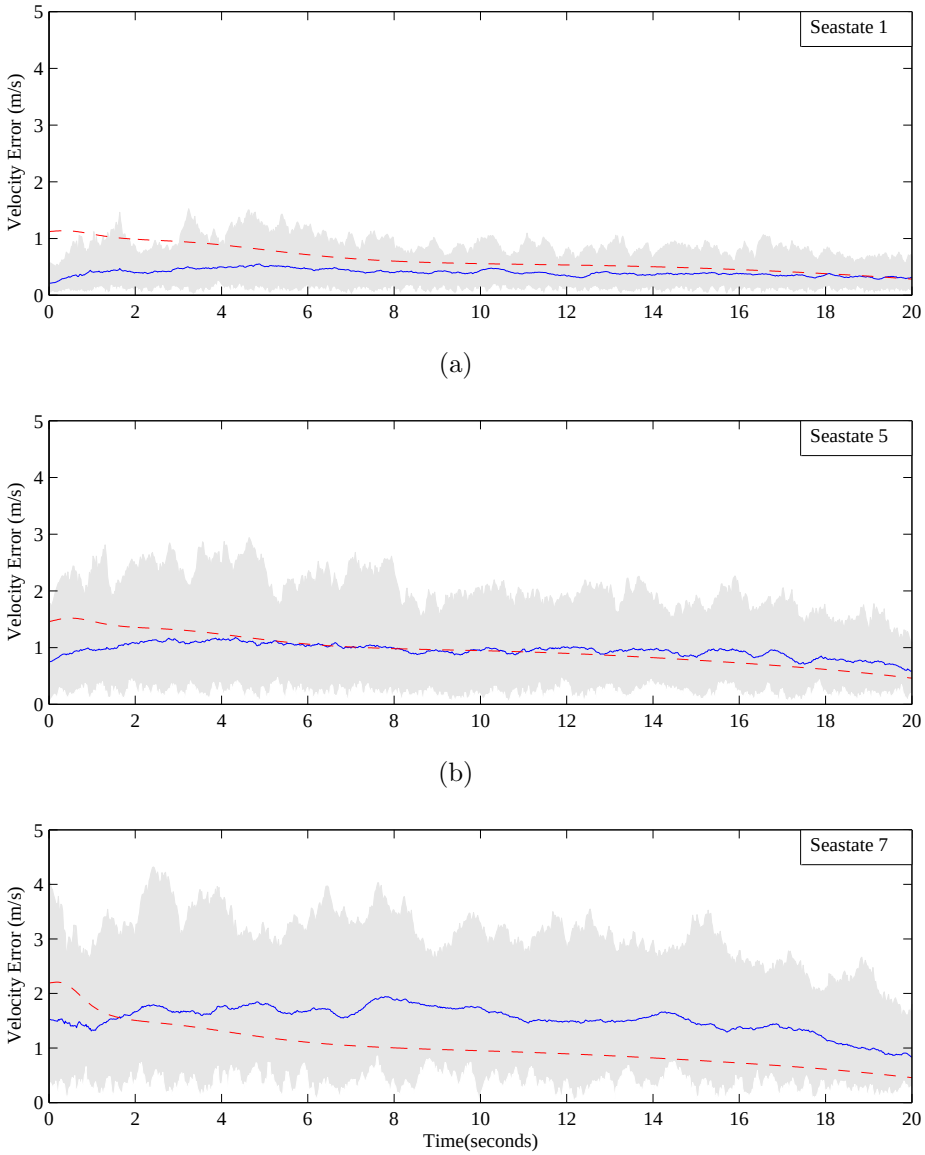

Figure 4.16. Velocity State Estimation Error vs. Sea state (Stochastic Wave Model) *Estimator velocity error for sea states 1, 5, 7. The grey region shows maximum and minimum bounds of true error. The blue line shows mean true error, and the red dashed line shows estimated total variance (i.e.* $\sqrt{\mathrm{Tr}\mathbf{P}}$*).*

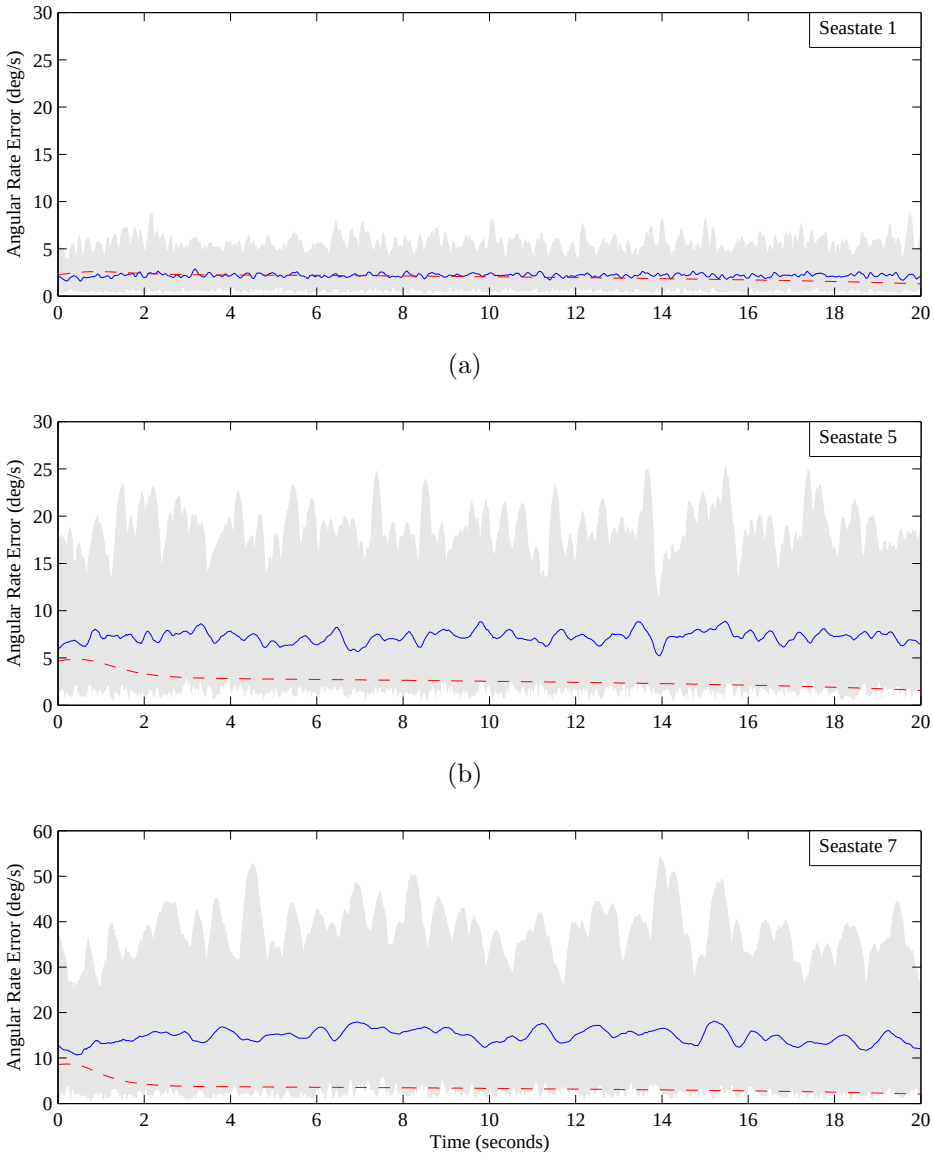

Figure 4.17. Angular Rate State Estimation Error vs. Sea state (Stochastic Wave Model)

Estimator angular rate error for sea states 1, 5, 7. The grey region shows maximum and minimum bounds of true error. The blue line shows mean true error, and the red dashed line shows estimated total variance (i.e. $\sqrt{\mathrm{Tr}\mathbf{P}}$*).*

4.5 Ferry Ship Motion Model

4.5.1 Representative Run Analysis (Fast Ferry Ship Model)

With the estimator shown to be able to estimate moderate wave motion for the previous two wave motion models, it is still important to attempt estimation using a model that was developed for ship motion specifically in order to further gain confidence in the results shown here.

Figure 4.18 shows the estimator again performing with accuracy when estimating ship deck position and orientation. This is consistent with the results from the other motion models. Final position error is 0.239 meters and final attitude error totals 0.682°.

Figure 4.19 shows the velocity and angular rate estimation of ship deck state versus time. The estimator does appear to lose accuracy in the velocity estimates, but only the vertical velocity estimates show data slightly outside of the covariance bounds. Attitude estimation is similar: while accuracy is diminished overall, the general motion is captured, and only yaw rate seems to escape the covariance bounds. Even with this diminished performance overall errors are small, totaling 0.201 meters per second for velocity and 0.682° per second for angular rate.

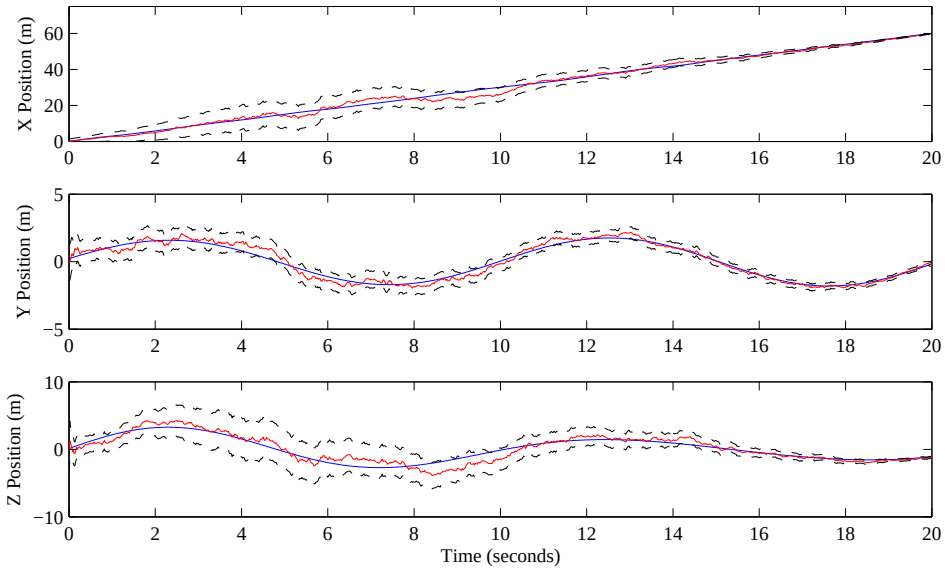

(a)

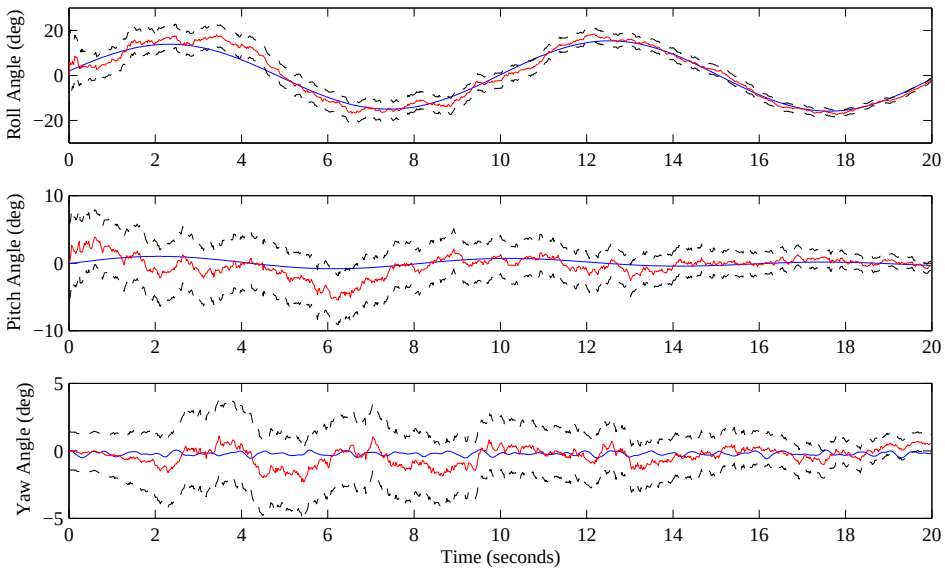

(b)

Figure 4.18. Representative Run Position and Orientation Estimation (Fast Ferry Ship Model)

Representative run position and orientation estimation using the fast ferry ship model. True state shown in blue, estimated state is shown in red, $\pm 2\sigma$ bounds are shown as dashed lines.

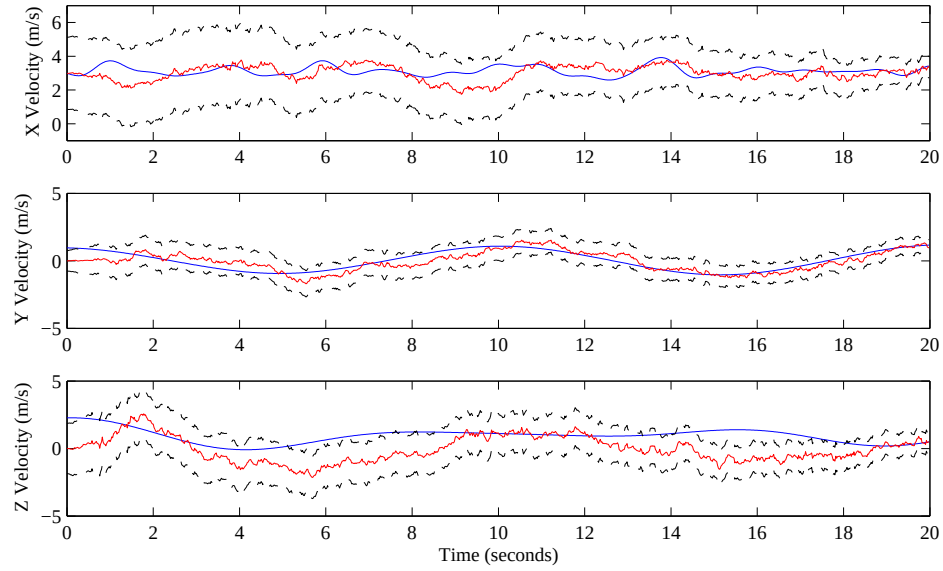

(a)

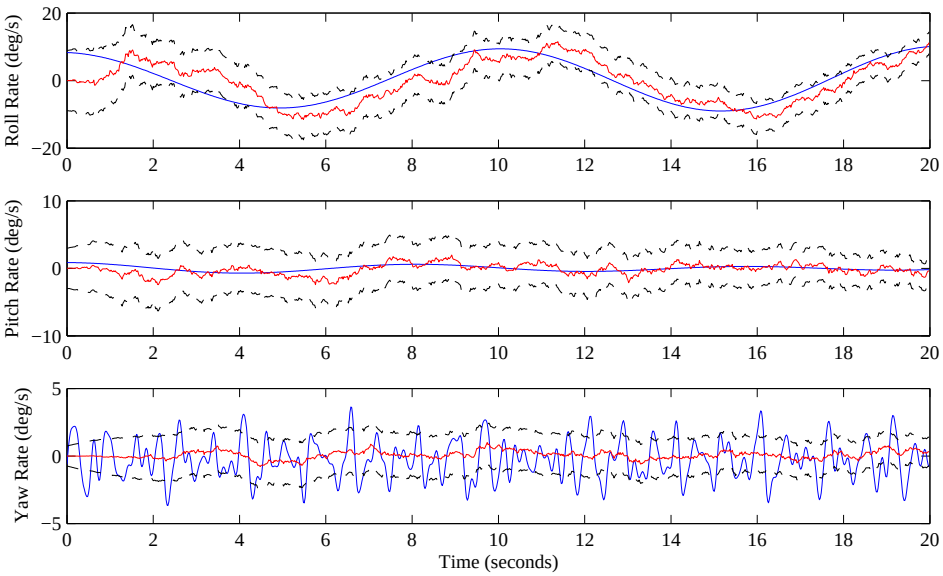

(b)

Figure 4.19. Representative Run Velocity and Angular Rate Estimation (Fast Ferry Ship Model)

Representative run position and orientation estimation using the fast ferry ship model. True state shown in blue, estimated state is shown in red, $\pm 2\sigma$ bounds are shown as dashed lines.

4.5.2 Monte Carlo Simulation Results (Fast Ferry Ship Model)

Figure 4.20 shows the total error estimation characteristics, as well as the error for each subset of deck states. Recall that this ship motion model is only described for "moderate wave motion" (sea state 4), and thus Monte Carlo results can only be shown for this sea state. Analysis of the overall estimation error shows a slight overconfidence by the estimator in the estimate at the end of the simulation. Figure 4.20(d) shows that this is caused by the velocity estimation error. All other state group errors are estimated to high precision, with no noticeable overconfidence from the estimator.

4.6 Summary

This chapter has presented several types of results involving estimation of ship deck motion undergoing several wave motion models and varying sea states.

1. Results from a deck undergoing a representative run with moderate wave motion were discussed. The average operation of the estimator in these conditions was shown. Results were gathered using two independent wave motion models as well as the ferry ship motion model.

    - The estimator was shown to perform accurately enough to operate in sea state conditions that other current autonomous landing systems would fail in.
    - Position and attitude state estimates are very accurately estimated for both motion models as well as the ship model.
    - Velocities and angular rates, while estimated adequately, were not tracked as precisely as the other deck states.

2. Estimator consistency was found versus varying sea states via results of Monte Carlo simulations.

    - The estimator was shown to consistently estimate positions to a high level of accuracy across sea states.

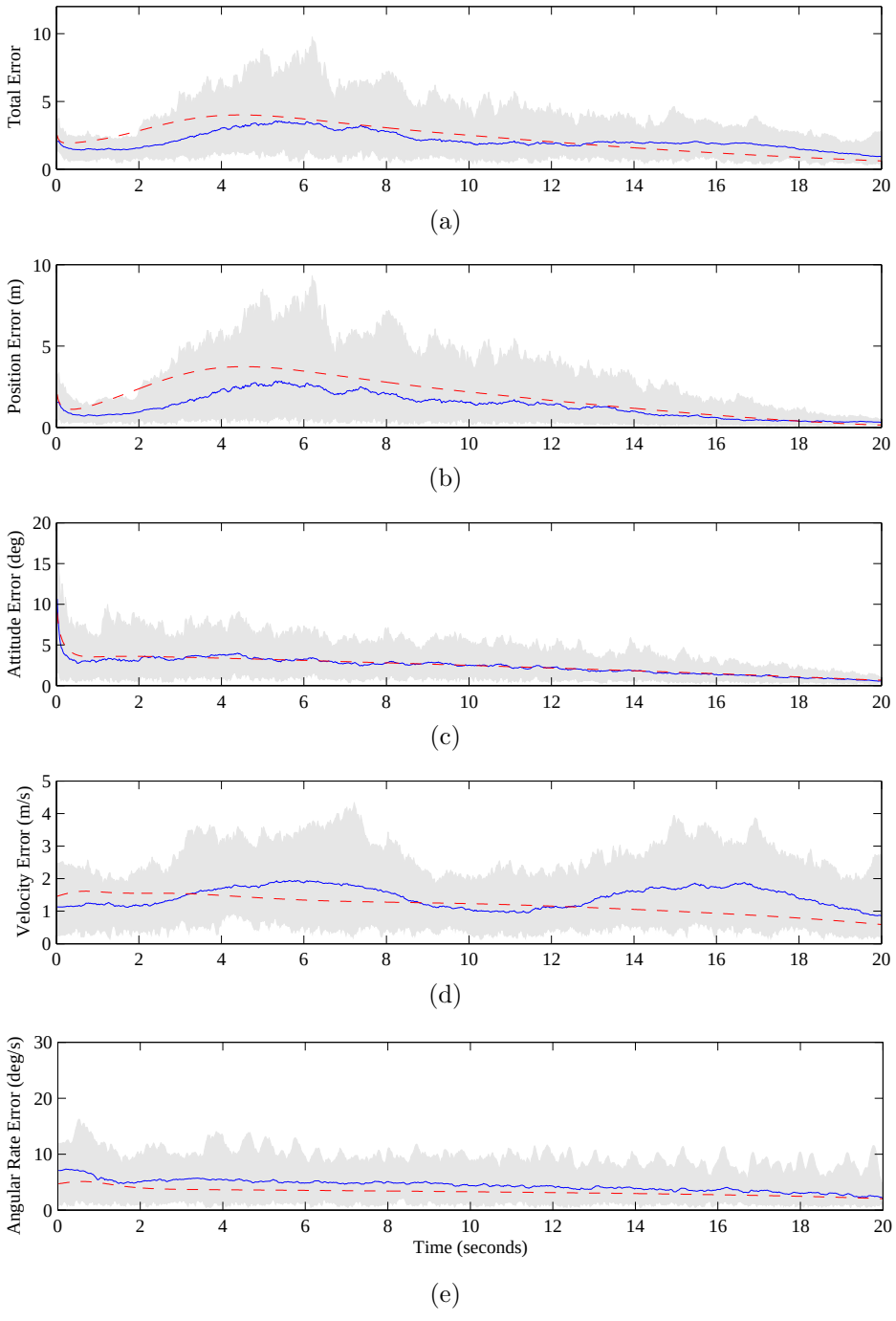

Figure 4.20. Deck State Estimation Error vs. Sea state (Fast Ferry Ship Model) *Estimator errors for sea state 4. The grey region shows maximum and minimum bounds of true error. The blue line shows mean true error, and the red dashed line shows estimated total variance (i.e.* $\sqrt{\mathrm{Tr}\mathbf{P}}$*).*

- The estimator was shown to have overconfidence in attitude estimation accuracy that correlated to increasing sea state, but this overconfidence was small.
- Deck velocities and rotation rates were shown to suffer from the same overconfidence issue. This is to be expected; since the deck has no measurement of deck velocity or rotation rates directly.

Chapter 5

Conclusion

This thesis was motivated by a lack of a generalized solution for an autonomous ship-board landing system. For manned aircraft, landing at sea can be a daunting challenge. To extend this capability to autonomous rotorcraft, especially smaller ones with limited capabilities, can only greatly increase the difficulty. Providing a simple, self-contained solution to this problem would greatly benefit military, civilian, and commercial use of these vehicles. Emergency operations, life threatening situations, and many other extreme theatres of operation could use autonomous vehicle capabilities to continuously provide support, supplies, or other aid.

While some solutions to this problem, such as Landing Period Designators and tether-based landing systems, do exist, they require specialized systems to enable landing operations. These systems can be expensive, faulty, and/or require extra crew maintenance to operate. In addition, the use of these systems limits UAV operation exclusively to ships outfitted with this technology.

This thesis envisions a self-contained system that requires as little alteration of the landing site as possible. The presented estimator only required that the ship transmit a single message defining sea state, ship heading and ship speed. The estimator assumes a 2^{nd} order kinematic model for deck motion. This is done with the intention to make this solution applicable across as wide a variety of ships and boats as possible. While the use of this second order kinematic model does result in some significant unmodeled dynamics, there is a significant advantage in the robustness of the resulting estimator to changes in deck motion dynamics; either from varying sea states or wave motion modeling techniques.

The goal of this research is to eventually provide a total system capable of: communication, observation, estimation, UAV control, and integrity monitoring. The research of this thesis has focused on the observation and estimation segments of the system. The individual contributions of this thesis are outlined in the following section. A solution with the capacity to accomplish all of these objectives has not been tested here, and much further research would need to be conducted to achieve total system capability. The necessary continued research to achieve these goals and to potentially improve overall performance is detailed in Section 5.2.

5.1 Summary of Contributions

5.1.1 Framework for Integrated Control and Navigation

An initial design for a framework which would facilitate integrated control and navigation of a small autonomous VTOL vehicle has been formed. The vehicle simulated only contained an IMU, GPS/INS, and low-cost commercially available vision measurement system. The solution presented addresses technical difficulties associated with deck state estimation using this sensor suite.

5.1.2 Estimator Design

An estimator utilizing an Unscented Kalman Filter was developed as a central piece of the control and navigation framework. The deck state vector is estimated using a known vehicle state and bearing measurements to fiducial, identical markers on the deck. Data association was performed based on a minimum cost correlation approach using the Munkres algorithm. The estimator computes an estimate of deck state (position, orientation, velocity, angular rate) and associated covariance. The deck state estimate can then be used by a landing trajectory planner.

5.1.3 Performance Verification: MATLAB Simulation

Both representative run and Monte Carlo simulations of a UAV approaching a moving deck display the capabilities of the estimator designed in this thesis. These analyses were performed for three distinct wave motion models (sinusoidal, stochas-

tic, and ferry), and the estimator was shown to perform adequately independent of which model was used. Monte Carlo simulations showed a small mean error when compared to overall wave influences for a variety of sea states. Only velocities and angular rates had less than ideal estimation characteristics; and these errors were small in magnitude and only occurred at higher sea states.

Representative run testing allowed for in depth performance into the actual expected performance of this estimator in sea state 5 conditions. State tracking for positions and attitudes was shown to be strong regardless of wave motion model. Knowledge of these states was good, as covariance bounds for the representative runs of these states converged significantly over the observation. Velocities and angular rates showed weaker, but still adequate, performance. However, this is to be expected, as the system has no way currently of measuring information about deck velocity and rotation rates.

The strength of performance was shown to hardly depend on the wave motion model used; as the more randomized motion of the stochastic model did not prove to be too complicated to estimate.

Overall this system is robust and capable of accurately estimating all deck states up to sea state 5, regardless of the deck motion model used. While position and attitude estimation at sea state 7 was accurate, velocity and attitude rate estimates did see degradation in results. While performance was not poor enough to consider this sea state a limit; this degradation could be mitigated by attempting to measure information about deck velocities, possibly via optical flow or some other method.

While performance of the system could be improved by specializing the estimator to a specific deck motion model or sea state, the results shown here indicate that performance of this generic model is more than adequate. The small gains in performance from a more specialized model are most likely outweighed by the broad applicability of the current system.

5.2 Recommendations for Future Work

5.2.1 Improved Marker Constellations

To this point all testing has been performed with markers placed on the corners of a square deck. Results of various marker orientations and outlines can be done in an attempt to enhance performance. Possibly setting up multiple marker arrays for different distances could help long distance and near landing estimation. Attaching markers to ship superstructure or on other parts of the ship may help with observability and improve performance of the estimation. Use of asymmetric marker outlines can be used as a stepping stone to far more varied, difficult landing setups, possibly culminating in unknown marker orientation testing.

5.2.2 More Accurate Wave Motion Models

Results from Chapter 4 have shown the performance of this estimator against several varied and complex wave and ship motion models, and for several different sea states. However, ship motion modeling is an ever-changing field as the types of ships, and accuracy of measurements evolves. As new motion models are developed, they should be tested against this estimator in order to confirm that its performance is at least adequate.

5.2.3 Improved Vision Information Processing

Future testing and use of physical cameras can lead to many potential issues with measuring marker bearings. As the complexity of the measurement model increases, updates to the vision measurement model must be performed. Potentially other information may be gleaned from the incoming data in order to perform faster, higher fidelity estimation. This may include utilizing vision interpretation properties like optical flow, or $\dot{\tau}$ (measuring optical flow of two points in frame relative to one another), which are techniques used by skilled flyers like birds and insects.

In addition, implementing more realistic (and possibly complex) measurement noise models can be done. This can further improve the realism of estimator performance. With this further complexity added to the vision system, it may be

deemed necessary to try and improve performance by including multiple cameras, or variable lenses for long and short range operation. This type of testing will be necessary before actual implementation, and would need to be done ensuring that the robustness and operation on small UAVS would not be compromised.

5.2.4 Observation Method

Another aspect of the simulation that could potentially be improved upon to yield better performance would be analysis of the observation method. For this thesis observation was performed as the vehicle descended and approached the deck from behind along a specified flight path angle. By incorporating more relative motion between the vehicle and deck, observability may increase, and this could lead to a faster decrease in state covariance as well as a better overall estimate of ship deck state. This approach path could include some sort of three-dimensional slalom, circling of the deck, or other complex motion. In order to accomplish this type of control, a more complex vehicle model would be needed. More analysis would be needed to determine the best possible approach for a given sea state and wave modeling technique; and whether the addition of a more complicated controller could cause any problems within the system.

5.2.5 Integrity Monitoring

Currently, there is no integrity monitoring taking place in the loop of simulation. All integrity analysis was performed manually after the completion of simulation. For a real autonomous system, this would need to be included in the control loop. This type of monitoring would insure that a collision was not imminent, and that the estimate of deck state was converging. This can all be accomplished through monitoring of the deck state estimate and covariance as they are currently formulated.

5.2.6 Further Hardware Testing

Much work has been put into a hardware system capable of real-time estimation of deck states using a single Chameleon 2 camera developed by Point Grey. This

system would be tested in a motion capture lab utilizing Cortex, motion capture software developed by Motion Analysis Corporation. The external motion capture software would be used in place of an internal INS/GPS system in order to provide vehicle states, and also would be used to determine true deck states for post-experiment results analysis.

Unfortunately networking problems between a machine running the motion capture software and another computer attempting to listen to the data being streamed out caused this research to be incomplete and left out of the thesis. Hopefully, this work can be continued. A successful real-time connection between the motion analysis software and an external computer running the simulation code detailed here could lead to a scale hardware setup where deck states are estimated accurately in real time.

Bibliography

[1] Robert H. Chen, Arthur Gevorkian, Alex Fung, Won-Zon Chen, and Vincent Raska, *Multi-sensor data integration for autonomous sense and avoid*, AIAA Infotech@Aerospace 2011 (St. Louis, Missouri), AIAA Paper 2011-1479, American Institute of Aeronautics and Astronautics, 29-31 March 2011.

[2] Bernard de Ferrier and T. Manning, *Simulation and testing of the landing period designator (lpd) helicopter recovery aid*, Naval Engineers Journal **110** (1998), no. 1, 189–205.

[3] David D. Diel, Paul DeBitetto, and Seth Teller, *Epipolar constraints for vision-aided inertial navigation*, IEEE Workshop on Motion and Video Computing, IEEE, 2005.

[4] Trevor Fitzgibbons and Eduardo Nebot, *Bearing only SLAM using colour-based feature tracking*, 2002 Australasian Conference on Robotics and Automation (Auckland, New Zealand), 2002.

[5] Eric W. Frew, Tristan Gerritsen, Stephen Pledgie, Chris Brinton, Shivang Patel, and Bonnie Schwartz, *Vision-based navigation for airfield surface operations*, AIAA Guidance, Navigation and Control Conference and Exhibit (Honolulu, Hawaii), AIAA Paper 2008-7320, American Institute of Aeronautics and Astronautics, August 18-21 2008.

[6] Ryan Gariepy and Steven L. Waslander, *Uav motion estimation using low quality image features*, AIAA Guidance, Navigation and Control Conference (Toronto, Ontario Canada), AIAA Paper 2010-8210, American Institute of Aeronautics and Astronautics, August 2010.

[7] Hiroyuki Hashimoto, Allen D. Wu, Girish Chowdhary, and Eric N. Johnson, *Avionics integration for a fully autonomous self-contained indoor miniature unmanned aerial system*, AIAA Infotech@Aerospace 2011 (St. Louis, Missouri), AIAA Paper 2011-1611, American Institute of Aeronautics and Astronautics, August 2011.

[8] Ronald A. Hess, *Simplified technique for modeling piloted rotorcraft operations near ships*, Journal of Guidance, Control and Dynamics **29** (2006), no. 6, 1339–1349.

[9] Gabriel M. Hoffmann, Steven L. Waslander, and Claire J. Tomlin, *Quadrotor helicopter trajectory tracking control*, AIAA Guidance, Navigation and Control Conference and Exhibit (Honolulu, Hawaii), AIAA Paper 2008-7410, American Institute of Aeronautics and Astronautics, August 18-21 2008.

[10] Inseok Hwang, Hamsa Balakrishnan, Kaushik Roy, and Claire Tomlin, *Multiple-target tracking and identity management with application to aircraft tracking*, Journal of Guidance, Control and Dynamics **30** (2007), no. 3, 641–653.

[11] Eric N. Johnson, Anthony J. Calise, Yoko Watanabe, Jincheol Ha, and James C. Neidhoefer, *Real-time vision-based relative navigation*, AIAA Guidance, Navigation and Control Conference and Exhibit (Keystone, Colorado), AIAA Paper 2006-6608, American Institute of Aeronautics and Astronautics, August 21-24 2006.

[12] Christopher G. Jones, Jacques J.F. Heyder-Bruckner, Thomas S. Richardson, and Chris D.C. Jones, *Vision-based control for unmanned rotorcraft*, AIAA Guidance, Navigation and Control Conference and Exhibit (Keystone, Colorado), AIAA Paper 2006-6684, American Institute of Aeronautics and Astronautics, August 21-24 2006.

[13] Andreas Koch, Hauke Wittich, and Frank Thielecke, *A vision-based navigation algorithm for a vtol-uav*, AIAA Guidance, Navigation and Control Conference and Exhibi (Keystone, Colorado), AIAA Paper 2006-6546, American Institute of Aeronautics and Astronautics, August 21-24 2006.

[14] Harold W. Kuhn, *The hungarian method for the assignment problem*, Naval Research Logistics Quarterly (Bryn Mawr, PA), 1955.

[15] Jack W. Langelaan, *State estimation for autonomous flight in cluttered environments*, Journal of Guidance, Control and Dynamics **30** (2007), no. 5, 1414–1426.

[16] Jacob W. Langelaan, *State estimation for autonomous vehicles in cluttered environments*, Ph.D. thesis, Stanford University, Stanford, California, 2006.

[17] Daniel Mellinger, *Trajectory generation and control for quadrotors*, Ph.D. thesis, University of Pennsylvania, Philadelphia, Pennsylvania, 2012.

[18] P. Travis Millet, Bryce B. Ready, and Timothy W. McLain, *Vision-based precision landings of a tailsitter uav*, AIAA Guidance, Navigation and Control Conference (Chicago, Illinois), AIAA Paper 2009-5680, American Institute of Aeronautics and Astronautics, August 10-13 2009.

[19] José Neira and Juan D. Tardós, *Data association in stochastic mapping using the joint compatibility test*, IEEE Transactions on Robotics and Automation **17** (2001), no. 6, 890–897.

[20] J. Nieto, J. Guivant, E. Nebot, and S. Thrun, *Real time data association for fastSLAM*, IEEE International Conference on Robotics and Automation (ICRA) (Taipei, Taiwan), IEEE, 2003, pp. 412–418.

[21] So-Ryeok Oh, Kasustubh Pathak, Sunil K. Agrawal, Hemanshu Roy Pota, and Matt Garratt, *Approaches for a tether-guided landing of an autonomous helicopter*, IEEE Transactions on Robotics **22** (2006), no. 3, 189–205.

[22] Tristan Pérez and Mogens Blanke, *Simulation of ship motion in seaway*, Technical report ee02037, The University of Newcastle, Australia and Technical University of Denmark, 2002.

[23] Alison Proctor and Eric N. Johnson, *Vision-only approach and landing*, AIAA Guidance, Navigation and Control Conference (San Francisco, California), AIAA Paper 2005-5871, American Institute of Aeronautics and Astronautics, August 2005.

[24] Katherine Ann Rink, *Use of the auction algorithm for target-object map*, AIAA **12** (1998), 709–719.

[25] Yassir Rizwan, Steven L. Waslander, and Christopher Nielsen, *Nonlinear aircraft modeling and controller design for target tracking*, American Control Conference (San Francisco, California), 2011 American Control Conference, June 29-July 01 2011.

[26] Srikanth Saripalli, James F. Montgomery, and Gaurav S. Sukhatme, *Vision-based autonomous landing of an unmanned aerial vehicle*, International Conference on Robotics and Automation (Washington, D.C.), IEEE, May 2002, pp. 2799–2804.

[27] Srikanth Saripalli and Gaurav S. Sukhatme, *Landing a helicopter on a moving target*, IEEE International Conference on Robotics and Automation, IEEE, 2007, pp. 2030–2035.

[28] Ramachandra J. Sattigeri, Eric Johnson, Anthony J. Calise, and Jincheol Ha, *Vision-based target tracking with adaptive target state estimator*, AIAA Guidance, Navigation and Control Conference and Exhibit (Hilton Head, South

Carolina), AIAA Paper 2007-6828, American Institute of Aeronautics and Astronautics, August 20-23 2007.

[29] Syed Irtiza Ali Sha, Suresh Kannan, and Eric N. Johnson, *Motion estimation for obstacle detection and avoidance using a single camera for uavs/robots*, AIAA Guidance, Navigation and Control Conference (Toronto, Ontario Canada), AIAA Paper 2010-7569, American Institute of Aeronautics and Astronautics, August 2-5 2010.

[30] Michael J. Tribou, Adeel Akhtar, and Steven L. Waslander, *Relative position-based visual servoing control for quadrotors*, AIAA Guidance, Navigation and Control Conference (Minneapolis, Minnesota), AIAA Paper 2012-5049, American Institute of Aeronautics and Astronautics, August 13-16 2012.

[31] Rudolph van der Merwe and Eric A. Wan, *The square-root unscented kalman filter for state and parameter-estimation*, IEEE International Conference on Acoustics, Speech, and Signal Processing (Salt Lake City, UT), May 7-11 2001.

[32] Yoko Watanabe, Anthony J. Calise, and Eric N. Johnson, *Vision-based obstacle avoidance for uavs*, AIAA Guidance, Navigation and Control Conference and Exhibit (Hilton Head, South Carolina), AIAA Paper 2007-6829, American Institute of Aeronautics and Astronautics, August 20-23 2007.

[33] Yoko Watanabe, Eric N. Johnson, and Anthony J. Calise, *Vision-based guidance design from sensor trajectory optimization*, AIAA Guidance, Navigation and Control Conference and Exhibit (Keystone, Colorado), AIAA Paper 2006-6607, American Institute of Aeronautics and Astronautics, August 2006.

[34] ———, *Stochastically optimized monocular vision based guidance design*, AIAA Guidance, Navigation and Control Conference and Exhibit (Hilton Head, South Carolina), AIAA Paper 2007-6865, American Institute of Aeronautics and Astronautics, August 2007.

[35] ———, *Autonomous flight in gps-denied environments using monocular vision and inertial sensors*, AIAA Infotech@Aerospace 2010 (Atlanta, Georgia), AIAA Paper 2010-3510, American Institute of Aeronautics and Astronautics, August 2010.

[36] Thomas P. Webb, Richard J. Prazenica, Andrew J. Kurdila, and Rick Lind, *Vision-based state estimation for autonomous micro air vehicles*, Journal of Guidance, Control and Dynamics **30** (2007), no. 3, 816–827.

[37] Jr. Williard J. Pierson and Lionel Moskowitz, *A proposed spectral form for fully developed wind seas based on the similarity theory of s. a. kitaigorodskii*, Journal of Geophysical Research **69** (1964), no. 24, 5181–5190.

[38] Allen D. Wu, Eric N. Johnson, and Alison A. Proctor, *Vision-aided inertial navigation for flight control*, AIAA Guidance, Navigation and Control Conference (San Francisco, California), AIAA Paper 2005-5998, American Institute of Aeronautics and Astronautics, August 2005.

[39] Junho Yang, Dushyant Rao, Soon-Jo Chung, and Seth Hutchinson, *Monocular vision-based navigation in gps-denied riverine environments*, AIAA Infotech@Aerospace 2011 (St. Louis, Missouri), AIAA Paper 2011-1403, American Institute of Aeronautics and Astronautics, August 2011.